

Role of Alkali Metal Cation Size in the Energy and Rate of Electron Transfer to Solvent-Separated 1:1 [(M⁺)(Acceptor)] (M⁺ = Li⁺, Na⁺, K⁺) Ion Pairs

Vladimir A. Grigoriev, Danny Cheng, Craig L. Hill,* and Ira A. Weinstock*[†]

Contribution from the Department of Chemistry, Emory University, Atlanta, Georgia 30322

Received January 8, 2001

Abstract: The effect of cation size on the rate and energy of electron transfer to [(M⁺)(acceptor)] ion pairs is addressed by assigning key physicochemical properties (reactivity, relative energy, structure, and size) to an isoelectronic series of well-defined M⁺–acceptor pairs, M⁺ = Li⁺, Na⁺, K⁺. A 1e⁻ acceptor anion, **a**-SiV^{IV}W₁₁O₄₀⁵⁻ (**1**, a polyoxometalate of the Keggin structural class), was used in the 2e⁻ oxidation of an organic electron donor, 3,3',5,5'-tetra-*tert*-butylbiphenyl-4,4'-diol (BPH₂) to 3,3',5,5'-tetra-*tert*-butylidiphenylquinone (DPQ) in acetate-buffered 2:3 (v/v) H₂O/*t*-BuOH at 60 °C (2 equiv of **1** are reduced by 1e⁻ each to **1**_{red}, **a**-SiV^{IV}W₁₁O₄₀⁶⁻). Before an attempt was made to address the role of cation size, the mechanism and conditions necessary for kinetically well behaved electron transfer from BPH₂ to **1** were rigorously established by using GC–MS, ¹H, ⁷Li, and ⁵¹V NMR, and UV–vis spectroscopy. At constant [Li⁺] and [H⁺], the reaction rate is first order in [BPH₂] and in [**1**] and zeroth order in [**1**_{red}] and [acetate] (base) and is independent of ionic strength, μ . The dependence of the reaction rate on [H⁺] is a function of the constant, K_{a1} , for acid dissociation of BPH₂ to BPH⁻ and H⁺. Temperature dependence data provided activation parameters of $\Delta H^\ddagger = 8.5 \pm 1.4$ kcal mol⁻¹ and $\Delta S^\ddagger = -39 \pm 5$ cal mol⁻¹ K⁻¹. No evidence of preassociation between BPH₂ and **1** was observed by combined ¹H and ⁵¹V NMR studies, while pH (pD)-dependent deuterium kinetic isotope data indicated that the O–H bond in BPH₂ remains intact during rate-limiting electron transfer from BPH₂ and **1**. The formation of 1:1 ion pairs [(M⁺)(SiVW₁₁O₄₀⁵⁻)]⁺ (M⁺**1**, M⁺ = Li⁺, Na⁺, K⁺) was demonstrated, and the thermodynamic constants, K_{M1} , and rate constants, k_{M1} , associated with the formation and reactivity of each M⁺**1** ion pair with BPH₂ were calculated by simultaneous nonlinear fitting of kinetic data (obtained by using all three cations) to an equation describing the rectangular hyperbolic functional dependence of k_{obs} values on [M⁺]. Constants, $K_{M1_{red}}$, associated with the formation of 1:1 ion pairs between M⁺ and **1**_{red} were obtained by using K_{M1} values (from k_{obs} data) to simultaneously fit reduction potential ($E_{1/2}$) values (from cyclic voltammetry) of solutions of **1** containing varying concentrations of all three cations to a Nernstian equation describing the dependence of $E_{1/2}$ values on the ratio of thermodynamic constants K_{M1} and $K_{M1_{red}}$. Formation constants, K_{M1} , and $K_{M1_{red}}$, and rate constants, k_{M1} , all increase with the size of M⁺ in the order $K_{Li1} = 21 < K_{Na1} = 54 < K_{K1} = 65$ M⁻¹, $K_{Li1_{red}} = 130 < K_{Na1_{red}} = 570 < K_{K1_{red}} = 2000$ M⁻¹, and $k_{Li1} = 0.065 < k_{Na1} = 0.137 < k_{K1} = 0.225$ M⁻¹ s⁻¹. Changes in the chemical shifts of ⁷Li NMR signals as functions of [Li₅**1**] and [Li₆**1**_{red}] were used to establish that the complexes M⁺**1** and M⁺**1**_{red} exist as solvent-separated ion pairs. Finally, correlation between cation size and the rate and energy of electron transfer was established by consideration of K_{M1} , k_{M1} , and $K_{M1_{red}}$ values along with the relative sizes of the three M⁺**1** pairs (effective hydrodynamic radii, r_{eff} , obtained by single-potential step chronoamperometry). As M⁺ increases in size, association constants, K_{M1} , become larger as smaller, more intimate solvent-separated ion pairs, M⁺**1**, possessing larger electron affinities (q/r), and associated with larger k_{M1} values, are formed. Moreover, as M⁺**1** pairs are reduced to M⁺**1**_{red} during electron transfer in the activated complexes, [BPH₂, M⁺**1**], contributions of ion pairing energy (proportional to $-RT \ln(K_{M1_{red}}/K_{M1})$) to the standard free energy change associated with electron transfer, ΔG°_{et} , increase with cation size: $-RT \ln(K_{M1_{red}}/K_{M1})$ (in kcal mol⁻¹) = -1.2 for Li⁺, -1.5 for Na⁺, and -2.3 for K⁺.

Introduction

As is documented in numerous published reports, additions of electrolyte or salts to solutions of charged electron-acceptor complexes result in substantial changes in the rates of charge-transfer processes¹ or of electron-transfer oxidations of organic or inorganic substrates.^{2–10} For oxidations by negatively charged

acceptors, additions of alkali metal cations typically result in increases in reaction rates. Examples include reductions of

- (2) Stalnakar, N. D.; Solenberger, J. C.; Wahl, A. C. *J. Phys. Chem.* **1977**, *81*, 601–604.
- (3) Goodwin, J. A.; Stanbury, D. M.; Wilson, L. J.; Eigenbrot, C. W.; Scheidt, W. R. *J. Am. Chem. Soc.* **1987**, *109*, 2979–2991.
- (4) Doine, H.; Swaddle, T. W. *Inorg. Chem.* **1988**, *27*, 665–670.
- (5) Braga, T. G.; Wahl, A. C. *J. Phys. Chem.* **1989**, *89*, 5822–5828.
- (6) Murguia, M. A.; Wherland, S. *Inorg. Chem.* **1991**, *30*, 139–144.
- (7) Wherland, S. *Coord. Chem. Rev.* **1993**, *123*, 169–199.
- (8) Andrieux, C. P.; Robert, M.; Savéant, J.-M. *J. Am. Chem. Soc.* **1995**, *117*, 9340–9346.

[†]Visiting scientist at Emory University, 1996–2001. Permanent address: USDA Forest Service, Forest Products Laboratory, Madison, WI 53705.

(1) Chen, P.; Meyer, T. J. *Chem. Rev.* **1998**, *98*, 1439–1477.

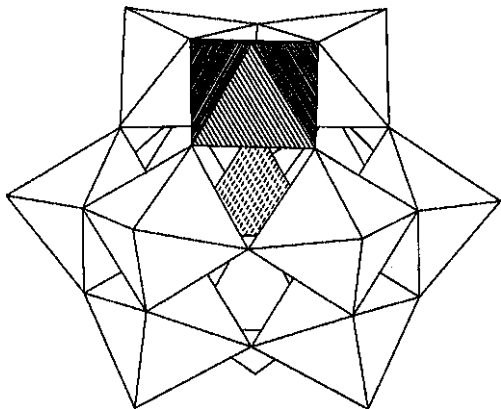


Figure 1. Drawing (in polyhedral notation) of α - $\text{SiVW}_{11}\text{O}_{40}^{5-}$ (1) where the central tetrahedron represents the $\text{Si}^{\text{V}}\text{O}_4$ unit, the shaded octahedron represents $\text{V}^{\text{V}}\text{O}_6$, and the unshaded octahedra represent $\text{W}^{\text{VI}}\text{O}_6$ units.

classical coordination complexes such as $\text{Mo}(\text{CN})_6^{3-}$,¹⁰ $\text{Fe}(\text{CN})_6^{3-}$,¹¹⁻¹⁴ $\text{Ru}(\text{CN})_6^{3-}$,¹⁵ $\text{Os}(\text{CN})_6^{3-}$,¹⁰ and IrCl_6^{3-} .¹⁵ Meanwhile, polyoxometalates¹⁶⁻¹⁹ (POMs), exemplified by α - $\text{SiVW}_{11}\text{O}_{40}^{5-}$ (1, a representative POM of the Keggin structural class; Figure 1), stand out as a large, rapidly growing, and increasingly useful class of anionic electron acceptors.^{20,21} As is true for solid-state structures or solutions of all such acceptor anions, countercations are always present. And, while uses of POMs in fundamental studies of metal oxide surfaces or in diverse applications from materials chemistry to catalysis continue to grow, the effects of countercations are largely ignored. However, in the few cases or systems in which cation effects have been assessed, their effects on synthesis and structure,²² on the nanoscale architecture and chemical properties of solid-state structures^{23,24} and on the chemistry of POM solutions^{20,21} have been substantial. In particular, the effects of alkali metal cations on energies and rates of electron transfer by POMs are central to the use of these anions as soluble oxidation or electron-transfer catalysts.²⁵

In general, this alkali metal cation catalysis is attributed to (1) association between the cation and the acceptor anion or (2) association of the cation with donor-acceptor complexes. In case 1, an increase in k_{obs} is attributed to a positive shift in the reduction potential of the acceptor complex upon cation

association. Indeed, numerous published reports document such positive shifts in reduction potential upon addition of alkali metal or alkaline earth cations to solutions of acceptor anions.^{14,26-29} In reference to case 2, it has been suggested that the cation facilitates preassociation, thus increasing the concentration of donor- M^+ -acceptor complexes that, in these instances, form prior to *intramolecular* electron transfer from donor to acceptor.²⁰ More generally, and applicable to either of the two cases (1 or 2), it has been argued that the cation present within donor- M^+ -acceptor complexes acts as an electronically more favorable pathway for electron transfer between donor and acceptor.^{10,11,20a}

Before the precise physicochemical role of the cation can be assessed, however, the extent and stoichiometry of ion association must first be determined. Only then can rate-accelerating effects arising from the structure and physical properties of specific M^+ -acceptor pairs or of ternary [donor, M^+ , acceptor] precursor complexes be rigorously established.^{7,30} For example, in polar, coordinating solvents, alkali metal cations typically accelerate rates of electron transfer to acceptor anions in the order $\text{Li}^+ < \text{Na}^+ < \text{K}^+$.¹⁰ This ordering, however, might be due (1) to differences in ion pair stoichiometries (e.g., 1:1 for Li^+ , giving [Li^+ -acceptor] association complexes, and higher-order (2:1 or 3:1) association complexes for Na^+ and K^+); (2) to greater association constants, K_{ip} , for stoichiometrically identical ion pairs (e.g., association constants for the formation of 1:1 ion pairs might increase in the order $\text{Li}^+ < \text{Na}^+ < \text{K}^+$); or (3) to the structure and physical properties of stoichiometrically identical donor- M^+ -acceptor precursor complexes (crystallographic radii increase in the order $\text{Li}^+ < \text{Na}^+ < \text{K}^+$). Three generic issues must thus be addressed in the study of specific cation catalysis of electron transfer: (1) the stoichiometry of ion pair formation; (2) the association constants, K_{ip} , for ion pairing; and (3) the physicochemical (structural and electronic) properties of specific M^+ -acceptor pairs. Only after stoichiometry (issue 1) has been established is it possible to differentiate between K_{ip} values (2) and the physical properties of specific M^+ -containing complexes (3). In labile reactive systems in particular, difficulties encountered in assigning precise stoichiometries to kinetically competent ion pairs or M^+ -containing association complexes have hampered efforts³¹ to separate trends in K_{ip} values from often parallel trends in physical properties of the reactive M^+ -containing complexes.

(25) For papers on electron donor/acceptor interactions in POM systems, many involving POMs and their countercations, see: (a) Prosser-McCartha, C. M.; Kadkhodayan, M.; Williamson, M. M.; Bouchard, D. A.; Hill, C. L. *J. Chem. Soc., Chem. Commun.* **1986**, 1747. (b) Williamson, M. M.; Bouchard, D. A.; Hill, C. L. *Inorg. Chem.* **1987**, *26*, 1436. (c) Schmidt, J. A.; Hilinski, E. F.; Bouchard, D. A.; Hill, C. L. *Chem. Phys. Lett.* **1987**, *138*, 346. (d) Hill, C. L.; Bouchard, D. A.; Kadkhodayan, M.; Williamson, M. M.; Schmidt, J. A.; Hilinski, E. F. *J. Am. Chem. Soc.* **1988**, *110*, 5471. (e) Le Maguerès, P.; Ouahab, L.; Golhen, S.; Grandjean, D.; Pena, O.; Jégaden, J. C.; Gómez-García, C. J.; Delhaès, P. *Inorg. Chem.* **1994**, *33*, 5180. (f) Ouahab, L. *Chem. Mater.* **1997**, *9*, 1909. (g) Attanasio, D.; Bonamico, M.; Fares, V.; Imperatori, P.; Suber, L. *J. Chem. Soc., Dalton Trans.* **1990**, 3221. (h) Zhang, X.-M.; Shan, B.-Z.; Bai, Z.-P.; You, X.-Z.; Duna, C.-Y. *Chem. Mater.* **1997**, *9*, 2687. (i) Le Maguerès, P.; Hubig, S. M.; Lindeman, S. V.; Veya, P.; Kochi, J. K. *J. Am. Chem. Soc.* **2000**, *122*, 10073-10082.

(26) Hanania, G. I. H.; Irvine, D. H.; Eaton, W. A.; George, P. J. *Phys. Chem.* **1967**, *71*, 2022-2030.

(27) Carloni, P.; Ebersson, L. *Acta Chem. Scand.* **1991**, *45*, 373-376.

(28) Boulas, P. L.; Gomez-Kaifer, M.; Echegoyen, L. *Angew. Chem., Int. Ed.* **1998**, *37*, 216-247.

(29) Beer, P. D.; Gale, P. A.; Chen, G. Z. *J. Chem. Soc., Dalton Trans.* **1999**, 1897-1910.

(30) In summarizing the effects of added electrolyte and ion pairing, Wherland (ref 7) concludes that, "study of the effects of ion pairing would be greatly facilitated if the structures, concentrations and lifetimes of ... ion paired species could be more directly evaluated ...".

(31) Ebersson, L. *J. Am. Chem. Soc.* **1983**, *105*, 3192-3199.

- (9) Fu, Y. S.; Swaddle, T. W. *Inorg. Chem.* **1999**, *38*, 876-880.
 (10) Metelski, P. D.; Swaddle, T. W. *Inorg. Chem.* **1999**, *38*, 301-307.
 (11) Shporer, M.; Ron, G.; Loewenstein, A.; Navon, G. *Inorg. Chem.* **1965**, *4*, 361-364.
 (12) Campion, R. J.; Purdie, N.; Sutin, N. *Inorg. Chem.* **1964**, *3*, 1091-1094.
 (13) Campion, R. J.; Deck, C. F.; King, P. J.; Wahl, A. C. *Inorg. Chem.* **1967**, *6*, 672-681.
 (14) Gritzner, G.; Danksagmüller, K.; Gutmann, V. *J. Electroanal. Chem.* **1976**, *72*, 177-185.
 (15) Hoddenbagh, J. M. A.; Macartney, D. H. *Inorg. Chem.* **1990**, *29*, 245-251.
 (16) Pope, M. T. *Heteropoly and Isopoly Oxometalates*; Springer-Verlag: Berlin, 1983.
 (17) Pope, M. T.; Müller, A. *Angew. Chem., Int. Ed. Engl.* **1991**, *30*, 34-48.
 (18) (a) Hill, C. L.; Prosser-McCartha, C. M. *Coord. Chem. Rev.* **1995**, *143*, 407-455. (b) Neumann, R. *Prog. Inorg. Chem.* **1998**, *47*, 317-370.
 (19) Hill, C. L., Guest Ed. Special Thematic Issue on Polyoxometalates. *Chem. Rev.* **1998**, *98*, 1-389.
 (20) (a) Saha, S. K.; Ali, M.; Banerjee, P. *Coord. Chem. Rev.* **1993**, *122*, 41-62. (b) Weinstock, I. A. *Chem. Rev.* **1998**, *98*, 113-170.
 (21) Grigoriev, V. A.; Hill, C. L.; Weinstock, I. A. *J. Am. Chem. Soc.* **2000**, *122*, 3544-45.
 (22) Kirby, J. F.; Baker, L. *Inorg. Chem.* **1998**, *37*, 5537-5543.
 (23) Misono, M. *Catal. Rev.-Sci. Eng.* **1987**, *29*, 269-321.
 (24) Mizuno, N.; Misono, M. *Chem. Rev.* **1998**, *98*, 199-218.

voltammetric analyzer. A three-electrode cell with a glassy carbon working electrode, a platinum auxiliary electrode, and a Ag/AgCl reference electrode was used. The sweep rate was 100 mV/s. No IR compensation was applied. Typically, **1** mM solutions of POM in a minimally (1 mM) acetate-buffered 2:3 (v/v) water/*t*-BuOH mixture (the water components were first adjusted to pH 4.76 by using HOAc and MOAc, M⁺ = Li⁺, Na⁺, or K⁺) were used. Cation concentrations were varied by adding the appropriate amounts of LiCl, NaCl, or KCl. Cyclic voltammetric measurements involving solutions containing tetra-*n*-hexylammonium (THA) cations (nitrate or POM salts) were carried out under Ar at 60 °C using a Ag/Ag⁺ reference electrode comprised of a Ag wire immersed in a solution of AgNO₃ (10 mM) and tetra-*n*-hexylammonium nitrate (THAN, 100 mM) in 2:3 (v/v) H₂O/*t*-BuOH.

Reaction kinetics data were collected by using electronic absorption spectroscopy (Hewlett-Packard 8451A diode array spectrometer). Two types of cuvettes were used for the kinetic experiments. For the reactions monitored for less than an hour (initial rate method), a quartz cuvette equipped with a stopcock sidearm and a standard taper 14/20 joint was used. The cuvette was filled with either POM or BPH₂ solution, and both the sidearm and the joint were sealed with rubber septum stoppers. POM solutions were degassed through the stopcock sidearm as liquids at 0 °C by applying three vacuum/argon cycles, and solid BPH₂ was degassed by using a freeze-pump-thaw procedure and stored under Ar. Next, the cuvette was placed in the sample compartment of the UV-vis spectrometer. This compartment was equipped with both a thermostat (±0.01 °C) and a stirrer. After thermal equilibration, the reaction was initiated by injecting BPH₂ (or POM) stock solutions into the POM (or BPH₂) solution with constant stirring at 800 rpm. For prolonged reactions (>1 h), a quartz cuvette with a stopcock sidearm and a Teflon stopper was used for better protection against gas leaks that could contribute to experimental error, especially at elevated temperatures. Both the degassing process and injection of the reactants were carried out through a rubber-septum-sealed sidearm. For prolonged reactions, however, the cuvette was tightly sealed with a Teflon stopper after the injection of the reactant.

Prior to use of UV-vis spectroscopy to obtain kinetic data, the extinction coefficient of a-Li₅SiV^{IV}W₁₁O₄₀ (Li₅I_{red}) at λ = 520 nm (though λ_{max} = 496 nm, the larger wavelength was used to monitor kinetics in order to minimize overlapping with tailing from the O²⁻ ⊗ W⁶⁺ charge-transfer band) was determined by linear regression by plotting the dependence of absorbance on POM concentration. A mixture of lithium-acetate-buffered aqueous solution (total concentration 0.25 M, pH 4.76) and *t*-BuOH (2:3, v/v) was used as the solvent. To avoid error due to liquid expansion upon heating, a series of solutions of Li₅I_{red} in the range 0.08–2 mM was prepared at 25 °C, and a second series of solutions was prepared at 60 °C. Measurements were taken using a quartz cuvette (path length = 1 cm) thermostated at either 25 or 60 °C with stirring (800 rpm).

Reaction Conditions and Product Analysis. The hydrophobic nature of the organic substrate and the highly hydrophilic nature of the POMs chosen for study required the use of a mixed aqueous-organic solvent system. Of the many solvent systems tested, the water/*t*-BuOH (2:3, v/v) mixture was found to be the most suitable for dissolving all reaction components over a wide range of concentrations. In a typical reaction, 0.02 mmol of Li₅**1** was dissolved in 4.0 mL of 0.1 M aqueous lithium acetate buffer solution (pH 4.76) in a 25-mL Schlenk flask. Next, 6.0 mL of *t*-BuOH was added, and the resulting solution was cooled to 0 °C. The cooled solution was degassed as a liquid by taking it through three vacuum/argon cycles. Using a gastight syringe, an aliquot (0.005–0.02 mmol) of degassed BPH₂ stock solution (0.06 M in *t*-BuOH) was injected through a septum into the flask charged with the POM solution, which was kept under Ar in a thermostated bath at 60 °C with constant stirring (800 rpm). After reaction times of 20–40 h, the Schlenk flask was removed from the bath, and the organic solvent (*t*-BuOH) and products were extracted using three 5-mL portions of CHCl₃. The POMs were insoluble in CHCl₃ and remained entirely in the buffered aqueous phase. Removal of the organic solvent by rotary evaporation afforded a solid residue that was dissolved in CDCl₃ for ¹H NMR measurements and GC-MS analysis (Hewlett-Packard 5890 gas chromatograph with a mass spectrometer detector). The yields of the organic products were

Table 1. Conversions and Product Yields for Oxidations of BPH₂ by **1**^a

[BPH ₂]:[1]	conversion of BPH ₂ (μmol) ^b	yield (μmol)		I _{red} (mmol)/DPQ (mmol)
		I _{red} ^c	DPQ ^b	
0.25:1.00 ^e	4.7±0.5	9.4±0.3	5.2±0.2	1.83±0.10
0.50:1.00 ^e	9.5±0.2	20.2±0.4	10.3±0.1	1.96±0.06
1.00:1.00 ^e	10.6±0.9	20.6±0.4	10.8±0.5	1.91±0.10

^a 20.0 μmol of Li₅**1**, 5.0–20.0 μmol of BPH₂, 20 mL of 0.1 M LiOAc/HOAc-buffered water/*t*-BuOH solution (2:3), pH 4.76, Ar, 60 °C. ^b Determined by ¹H NMR. ^c Determined by UV-vis spectroscopy at 520 nm (ε = 619 M⁻¹ cm⁻¹). ^d Reaction time of 40 h. ^e Reaction time of 20 h.

quantified by ¹H NMR using 3',4'-dichloroacetophenone as an internal standard. The aqueous solution that remained after extraction by CHCl₃ was transferred into a 25-mL volumetric flask, and water was added to obtain 25 mL of a POM solution of known concentration. The concentration of I_{red} present in the aqueous POM solution was determined by both UV-visible spectrometry (λ = 520 nm, ε = 619 cm⁻¹ M⁻¹) and oxidative titration using (NH₄)₂Ce^{IV}(NO₃)₆ as oxidant and primary standard and ferroin as an indicator.³⁵

Reaction Stoichiometry. In 2:3 (v/v) H₂O/*t*-BuOH at 60 °C, 3,3',5,5'-tetra-*tert*-butylbiphenyl-4,4'-diol (BPH₂) is cleanly oxidized by 2 equiv of a-SiVW₁₁O₄₀⁵⁻ (**1**) to 3,3',5,5'-tetra-*tert*-butyldiphenylquinone (DPQ, 100% by ¹H NMR and GC-MS; eq 1). The stoichiometry in eq 1 was established by quantitative spectroscopic (¹H NMR and UV-vis) analysis of percent conversions and product yields over a range of initial BPH₂-to-**1** ratios (Table 1). BPH₂ and DPQ are the only organic compounds observed by ¹H NMR. The percent conversion of **1** to its 1e⁻ reduction product, I_{red}, was determined by UV-vis spectroscopy at λ = 520 nm (ε = 619 M⁻¹ cm⁻¹). At each BPH₂-to-**1** ratio, 2 equiv of **1** is reduced to I_{red} (eq 1). No intermediates of partial oxidation of BPH₂ are observed.

Rate Expressions. Orders of reaction with respect to the concentrations of POM, (initially, fully oxidized **1**), BPH₂, POM_{red} (1e⁻-reduced POM, I_{red}), H⁺, and OAc⁻ (investigation of general base catalysis) and ionic strength (μ) were determined by using Li₅**1** and Li₅I_{red} in the lithium-acetate-buffered H₂O/*t*-BuOH (2:3, v/v) solvent system described above. All experiments were carried out under anaerobic conditions (Ar) at 60 °C.

Dependence of Rate on [1]. To determine the order of reaction with respect to the concentration of **1**, a stock solution of BPH₂ (0.06 M) in *t*-BuOH was prepared by using a 10-mL volumetric flask. The BPH₂ solution was transferred to a 10-mL round-bottom flask, which was then sealed with a rubber septum, degassed by several sequential freeze-pump-thaw cycles, and kept under Ar in a refrigerator. Solutions of Li₅**1** (0.38–5.6 mM) in a 0.1 M lithium-acetate-buffered H₂O/*t*-BuOH (2.2:2.8, v/v) mixture were prepared immediately prior to each experiment. Next, 2.7 mL of the POM solution was transferred by syringe to a Schlenk cuvette. The solution was degassed as a liquid as described above, and the cuvette was then placed in the UV-vis spectrometer. The reaction was initiated by injecting 0.3 mL of the BPH₂ stock solution into the POM solution. Dilution resulting from injection of stock BPH₂ solution was taken into account, and concentrations of all reaction components were calculated accordingly ([Li₅**1**]₀ = 0.34–5.0 mM, [LiOAc] = 0.10 M, H₂O/*t*-BuOH = 2:3, v/v).

Dependence of Rate on [BPH₂]. To determine the dependence of the reaction rate on BPH₂ concentration, a stock solution of Li₅**1** (0.06 M) in 0.25 M lithium-acetate-buffered water (pH 4.76) was prepared in a 10-mL volumetric flask, transferred into a 25-mL round-bottom flask, degassed as a liquid, and filled with Ar. Next, 1.8 mL of BPH₂ solution (0.5–10 mM) in *t*-BuOH and 1.2 mL of 0.25 M lithium acetate buffer solution in water (pH 4.76) were transferred by syringe into a Schlenk cuvette and degassed at 0 °C by using the freeze-pump-thaw procedure. The reaction was initiated by injecting 20 μL of the POM stock solution into the BPH₂ solution.

Dependence of Rate on [I_{red}]. The procedure was identical to that used to determine the order of reaction with respect to [**1**] except that

(35) Kolthoff, I. M.; Sandell, E. B.; Meehan, E. J.; Bruckenstein, S. *Quantitative Chemical Analysis*, 4th ed.; Macmillan: London, 1969; p 817.

0–40 μL of $\text{Li}_5\mathbf{1}_{\text{red}}$ stock solution (0.24 M) in 0.1 M lithium-acetate-buffered $\text{H}_2\text{O}/t\text{-BuOH}$ (2:3, v/v) solvent system was injected into the solution of $\text{Li}_5\mathbf{1}$ before degassing.

Dependence of Rate on [OAc]. LiOAc/HOAc buffer concentrations were varied while keeping the ionic strength constant. Lithium-acetate-buffered solutions with $\text{pH } 4.76 \pm 0.01$ and concentrations of LiOAc from 0.010 to 0.200 M were used. The aqueous buffer solutions were combined with $t\text{-BuOH}$ (2:3, v/v), and the mixtures were used for the reactions of $\text{Li}_5\mathbf{1}$ with BPH_2 . LiCl was added to the aqueous buffer solutions to keep the final $[\text{Li}^+]$ and ionic strength constant (0.200 M). The order of the reactant addition was the same as that used to determine the dependence of the reaction rate on [POM].

Dependence of Rate on Ionic Strength. To establish the dependence of the reaction rate on the ionic strength at constant cation (Li^+) concentration, the ionic strength was varied by adding appropriate amounts of LiCl or $\alpha\text{-LiAl}(\text{AlOH}_2)\text{W}_{11}\text{O}_{39}$ ($\text{Li}_6\mathbf{2}$). First, solutions of LiCl (10.2 mM) and $\text{Li}_6\mathbf{2}$ (1.6 mM) in the 1 mM lithium-acetate-buffered $\text{H}_2\text{O}/t\text{-BuOH}$ (2:3, v/v) solvent system were prepared. Solutions of $\text{Li}_5\mathbf{1}$ (1.0 mM) were prepared by using each of those (LiCl or $\text{Li}_6\mathbf{2}$) solutions. The concentrations of Li^+ in both solutions were very similar (13.1 mM Li^+ in LiCl-containing solutions and 12.5 mM in $\text{Li}_6\mathbf{2}$ solutions), whereas their ionic strengths differed substantially (16.9 and 40.4 mM, respectively). The procedure then followed was identical to that used to determine the order of reaction with respect to [1], except that 100- μL aliquots of 0.06 M BPH_2 stock solution were injected.

Reaction Rates. Reaction rate kinetics were measured by recording the absorbance at 520 nm (ϵ for $\alpha\text{-SiVU}^{10}\text{W}_{11}\text{O}_{40}^{6-}$, $\epsilon = 619 \text{ M}^{-1} \text{ cm}^{-1}$) once every 2–200 s (depending on the experiment) for 0.5–20 h. For determination of the order of reaction, the timer was started when the reaction was initiated (injection of BPH_2 or POM) and was controlled by the Time-Based Measurement in the HP UV-Visible Chemstation General Scanning Software, which took automatic measurements at set times. The rate law, kinetic isotope effect, and activation parameters were calculated from absorbance versus time data by using the initial rate method (POM conversion <5%). The dependence of the reaction rate on the nature of the cation (i.e., Li^+ , Na^+ , and K^+) was determined by using the initial rate method. At least three reproducible measurements of reaction rate (or rate constant) were obtained for every experiment. The absence of a dependence of reaction rate on the concentration of the effectively nonpairing cation, tetra-*n*-hexylammonium (THA, present as counterion in $\text{THA}_5\mathbf{1}$ and THAN), was demonstrated by using the initial rate method.

Kinetic Model. An expression for the time dependence of the reaction rate (the rate of formation of $\mathbf{1}_{\text{red}}$) was derived from the experimentally determined rate law (applicable to pH values <5):

$$\frac{d[\mathbf{1}_{\text{red}}]}{dt} = k_{\text{obs}}[\mathbf{1}][\text{BPH}_2] \quad (3)$$

Taking into account the stoichiometry of the reaction (eq 1), the following kinetic model was derived (the full derivation is included in the Supporting Information):

$$[\mathbf{1}_{\text{red}}]_t = [\mathbf{1}]_0 - \frac{[\text{BPH}_2]_0 - \frac{[\mathbf{1}]_0}{2}}{[\text{BPH}_2]_0 \exp\left[k_{\text{obs}}\left([\text{BPH}_2]_0 - \frac{[\mathbf{1}]_0}{2}\right)t\right] - \frac{1}{2}} \quad (4)$$

where $[\mathbf{1}]_0$ and $[\text{BPH}_2]_0$ are initial concentrations of $\mathbf{1}$ and BPH_2 , respectively, and $[\mathbf{1}_{\text{red}}]_t$ is the concentration of $\mathbf{1}_{\text{red}}$ at time t .

To determine the second-order rate constant from absorbance versus time data by using eq 4, the data were fitted directly to the full second-order rate equation:

$$A_t = \epsilon \left\{ [\mathbf{1}]_0 - \frac{[\text{BPH}_2]_0 - \frac{[\mathbf{1}]_0}{2}}{[\text{BPH}_2]_0 \exp\left[k_{\text{obs}}\left([\text{BPH}_2]_0 - \frac{[\mathbf{1}]_0}{2}\right)t\right] - \frac{1}{2}} \right\} + A_0 \quad (5)$$

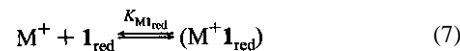
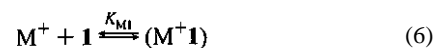
where $[\mathbf{1}]_0$ and $[\text{BPH}_2]_0$ are the same as in eq 4, and A_0 and A_t are the initial absorbance and the absorbance at time t , respectively. Nonlinear least-squares fitting of the absorbance versus time data was performed by using the Solver Function in Microsoft Excel 98. Sums of the squares of the deviation were minimized by varying one (k_{obs}) or two (k_{obs} and ϵ) parameters. Though ϵ was experimentally determined by using an independent technique as described above, a small experimental uncertainty in the independently obtained value was present. Therefore, both k_{obs} and ϵ were allowed to vary. Significantly, however, final values for ϵ obtained by nonlinear two-parameter fitting differed by less than 0.5% from the independently obtained experimental value.

pH Measurements. pH values in both water and water/ $t\text{-BuOH}$ mixtures were measured by using a Coming Bench-Top pH meter, model 240, equipped with a Coming Semi-Micro Combination electrode. If not otherwise noted, pH values presented are those of the aqueous acetate buffer solutions (pH = 3.90–5.76) measured before mixing with $t\text{-BuOH}$. For experiments designed to assess the pH dependence of the rate constant, pH values were measured directly in water/ $t\text{-BuOH}$ mixtures just prior to initiation of reaction. Because of gradual drifting of pH meter readings in the mixed-solvent system, a careful measuring protocol was used.³⁶ First, the pH meter (glass electrode) was calibrated by using typical aqueous standards (pH 4.00 and 7.00). Next, the glass electrode was immersed in the mixed-solvent solution, the electrode was left to equilibrate for 2 min, and three readings were taken, one immediately and the next two after 2-min intervals. The average of the three readings was used as the apparent pH value.

Kinetic Isotope Effect. The reaction conditions and reactant addition protocols were identical to those described above (e.g., in determination of the order of reaction with respect to [1]) except that the initial concentrations of BPH_2 and $\text{Li}_5\mathbf{1}$ were 2.86 and 0.48 mM, respectively. To determine k_{D} = $(d[\mathbf{1}_{\text{red}}]/dt)_{\text{D}}/([\mathbf{1}], [\text{BPD}_2]_0)$, the solvent system $\text{D}_2\text{O}/t\text{-BuOD}$ (2:3, v/v) was used. All other components (0.1 M HOAc, 2.86 mM BPH_2 , and 0.48 mM $\text{Li}_5\mathbf{1}\cdot 12\text{H}_2\text{O}$), which may have contributed <0.3% of labile hydrogen atoms versus >99.7% of labile deuterium atoms from D_2O (44.3 M) and $t\text{-BuOD}$ (6.4 M), were nondeuterated. Given the low concentration of BPH_2 and the fast exchange between D^+ in D_2O and H^+ in the hydroxyl groups of BPH_2 , deuterated BPH_2 (i.e., BPD_2) is generated in situ on a time scale much faster than that of the redox reaction under investigation. Because the reaction rate was found to be pH-dependent, it was important to use H_2O and D_2O buffer solutions that possessed the same $[\text{H}^+]$ and $[\text{D}^+]$ values, respectively. To prepare buffer solutions in D_2O , ordinary aqueous standards were used to calibrate the pH meter, and pH readings were corrected to give pD values according to the equation,^{37,38} $\text{pH}_{\text{obs}} = \text{pD} - 0.40$, where pH_{obs} is the observed pH value (pH meter reading) and pD is the true pD value.

Cation–Anion Pairing Studies. Ion pairing between alkali metal cations and POMs in solution was studied by determining the effect of the nature of the cation and its concentration on the observed rate constant for oxidation of BPH_2 by POM and on the formal redox potential of the POM solutions, and by ^7Li NMR.

The following assumption was used to derive the functional dependencies of both the observed rate constant and the POM redox potential on cation concentration: $\mathbf{1}$ and $\mathbf{1}_{\text{red}}$ are in rapid equilibrium with the corresponding cation–POM ion pairs (eqs 6 and 7).



The thermodynamic equilibrium constants for ion pairing are defined by the equations

(36) Cohen, L. A.; Jones, W. M. *J. Am. Chem. Soc.* 1963, 85, 3397.

(37) Westcott, C. C. *pH Measurements*; Academic Press: New York, 1978; p 85.

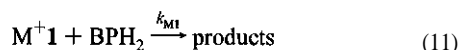
(38) Covington, A. K.; Paabo, M.; Robinson, R. A.; Bates, R. G. *Anal. Chem.* 1968, 40, 700–706.

$$K_{M1} = \frac{[M^+1]\gamma'_{ox}}{[M^+]\gamma_M[1]\gamma_{ox}} \quad (8)$$

$$K_{M1_{red}} = \frac{[M^+1_{red}]\gamma'_{red}}{[M^+]\gamma_M[1_{red}]\gamma_{red}} \quad (9)$$

The activity coefficients, g_{ox} , g'_{ox} , g_{red} , g'_{red} , and g_M , corresponding to unpaired and paired **1**, **1_{red}**, and M⁺ ions, had to be used in order to correct for nonideal behavior due to significant changes in ionic strength (μ) upon varying the cation concentration,

An expression describing the reaction rate ($d[\text{a-SiV}^{\text{IV}}\text{W}_{11}\text{O}_{40}^{6-}]/dt$ or $d[1_{red}]/dt$) and the dependence of the observed rate constant on [M⁺], consistent with the proposed mechanism of oxidation of BPH₂ by **1**, was derived by using eqs 10–12:



$$\text{rate} = k_1[1]\gamma_{ox}[\text{BPH}_2]\gamma_o + k_{M1}[M^+1]\gamma'_{ox}[\text{BPH}_2]\gamma_o \quad (12)$$

where g_o is the activity coefficient for BPH₂. Use of the definition of K_{M1} (eq 8) and rearrangement (eqs 13–15) gives eq 16.

$$\text{rate} = k_1[1]\gamma_{ox}[\text{BPH}_2]\gamma_o + k_{M1}K_{M1}[M^+]\gamma_M[1]\gamma_{ox}[\text{BPH}_2]\gamma_o \quad (13)$$

$$\text{rate} = (k_1 + k_{M1}K_{M1}[M^+]\gamma_M)[1][\text{BPH}_2]\gamma_{ox}\gamma_o \quad (14)$$

$$\text{rate} = (k_1 + k_{M1}K_{M1}[M^+]\gamma_M) \frac{[1][\text{BPH}_2]\gamma_{ox}\gamma_o}{[1] + [M^+1]} \quad (15)$$

$$\text{rate} = (k_1 + k_{M1}K_{M1}[M^+]\gamma_M) \frac{[\text{BPH}_2]\gamma_{ox}\gamma_o}{1 + K_{M1}[M^+]\gamma_M \frac{\gamma_{ox}}{\gamma'_{ox}}} \frac{[1]}{[1] + [M^+1]} \quad (16)$$

Substitution of initial rate (rate_o) and initial reactant concentrations ([**1**], and [BPH₂]_o) gives

$$\text{rate}_o = \frac{k_1 + k_{M1}K_{M1}[M^+]\gamma_M}{1 + K_{M1}[M^+]\gamma_M \frac{\gamma_{ox}}{\gamma'_{ox}}} [1]_o [\text{BPH}_2]_o \gamma_{ox} \gamma_o \quad (17)$$

From eq 17, the dependence of the observed rate constant on cation concentration is a rectangular hyperbolic function:

$$k_{obs} = \frac{k_1 + k_{M1}K_{M1}[M^+]\gamma_M}{1 + K_{M1}[M^+]\gamma_M \frac{\gamma_{ox}}{\gamma'_{ox}}} \gamma_{ox} \gamma_o \quad (18)$$

The dependence of the V_{1/2} half-wave potentials on the cation concentration was analyzed by using a Nernstian equation modified to include two ion pairing constants (by convention, $K_{ox} = K_{M1}$ and $K_{red} = K_{M1_{red}}$).³⁹

$$E_{1/2} = E^\circ + \frac{RT}{nF} \ln \left(\frac{1 + K_{red} \frac{\gamma_M \gamma_{red}}{\gamma'_{red}} [M^+]}{1 + K_{ox} \frac{\gamma_M \gamma_{ox}}{\gamma'_{ox}} [M^+]} \right) + \frac{RT}{nF} \ln \frac{\gamma_{ox}}{\gamma_{red}} \quad (19)$$

where E° is the standard potential for unpaired **1** at zero ionic strength, μ , and the other symbols are conventional or described above.

(39) Butler, J. N.; Cogley, D. R. *Ionic Equilibrium: Solubility and pH Calculations*; John Wiley & Sons: New York, 1998; pp 332–333.

The activity coefficients in both eqs 18 and 19 were calculated by using the extended Debye–Hückel law with a linear empirical correction term:⁴⁰

$$\log \gamma_z = -Az^2 \frac{\sqrt{\mu}}{1 + Ba\sqrt{\mu}} + b\mu \quad (20)$$

where g_2 is the activity coefficient of a singleion of charge z , a (1.825 $10^6(\text{eT})^{-1/2} \text{ mol}^{-1/2} \text{ L}^{1/2} \text{ K}^{3/2}$) and B (50.29 $(\text{eT})^{-1/2} \text{ \AA}^{-1} \text{ mol}^{-1/2} \text{ L}^{1/2} \text{ K}^{1/2}$) are constants that depend on the temperature and the dielectric constant of the solvent, and a and b are adjustable parameters.

Both kinetic and electrochemical data were fitted to eqs 18 and 19, respectively. Nonlinear least-squares fits of the observed rate constant and the formal redox potential versus cation concentration were performed by using the Solver Function in Microsoft Excel 98. Sums of the squares of the deviations were minimized by varying parameters k_{ox} , k_1 , K_{ox} , K_{red} , E_o , a , and b in eqs 18–20. The ratios g_{ox}/g'_{ox} and g_{red}/g'_{red} were assumed to be 1. The limitations and constraints that were imposed on the adjustable parameters to improve fitting are discussed below.

⁷Li NMR Studies of Ion Pairing. Solutions of Li₅**1** (0.3–20 mM) or Li₆**1_{red}** (0.5–10mM) in 23 H₂O/*t*-BuOH were prepared at 60.0 °C. A coaxial insert filled with 1.0 M LiCl in D₂O was used as an external reference. The samples were allowed to warm to 60 °C in the NMR probe for at least 10 min prior to initiation of spectral acquisition. The NMR spectra were recorded with a digital resolution of 0.061 Hz (0.0004 ppm).

The following experimentally verified solution behavior established boundary conditions used in derivation of a functional dependence of the observed chemical shift on the total concentration of Li₅**1** ([Li₅**1**]_{total}):

(1) In very dilute solutions, Li₅**1** is completely dissociated into Li⁺ and **1**.

(2) At larger [Li₅**1**] (within the experimental limits), ion pairing occurs according to eq 21,



where K_{Li1} (identical to analogous constants in eqs 8, 18, and 19) is the association constant defined by eq 22,

$$K_{Li1} = \frac{[\text{Li}\mathbf{1}]\gamma_{Li1}}{[\text{Li}^+][\mathbf{1}]\gamma_{Li}\gamma_1} \quad (22)$$

and the mass balance for Li⁺- and **1**-containing species is defined by equations

$$5[\text{Li}_5\mathbf{1}]_{\text{total}} = [\text{Li}^+] + [\text{Li}\mathbf{1}] \quad (23)$$

$$[\text{Li}_5\mathbf{1}]_{\text{total}} = [\mathbf{1}] + [\text{Li}\mathbf{1}] \quad (24)$$

(3) Solvated Li⁺ cations, both free and associated, undergo rapid exchange on the ⁷Li NMR time scale. Thus, the observed chemical shift (δ) is the weighted mean of the chemical shifts of the signals due to unpaired (δ_o) and paired (δ_1) Li⁺ ions.^{41–43}

$$\delta = \delta_o \frac{[\text{Li}^+]}{5[\text{Li}_5\mathbf{1}]_{\text{total}}} + \delta_1 \frac{[\text{Li}\mathbf{1}]}{5[\text{Li}_5\mathbf{1}]_{\text{total}}} \quad (25)$$

Using eq 23, eq 25 is rewritten as

(40) Robinson, R. A.; Stokes, R. H. *Electrolyte Solutions*; Butterworth: London, 1959; p 231.

(41) McCormick, A. V.; Bell, A. T.; Radke, C. J. *J. Phys. Chem.* **1989**, *93*, 1733–1737.

(42) Akai, T.; Nakamura, N.; Chihara, H. *J. Chem. Soc., Faraday Trans.* **1993**, *89*, 1339–1343.

(43) Kabisch, G. *Ber. Bunsen-Ges. Phys. Chem.* **1982**, *86*, 636.

$$\delta = \delta_0 + (\delta_1 - \delta_0) \frac{[\text{Li}\mathbf{1}]}{5[\text{Li}_5\mathbf{1}]_{\text{total}}} \quad (26)$$

An expression for the concentration of paired species, $[\text{Li}\mathbf{1}]$, as a function of the total concentration of $\text{Li}_5\mathbf{1}$ and the association constant, $K_{\text{Li}\mathbf{1}}$ was derived by using the definition of $K_{\text{Li}\mathbf{1}}$ (eq 22) and both mass balance eqs 23 and 24:

$$[\text{Li}\mathbf{1}] = 3[\text{Li}_5\mathbf{1}]_{\text{total}} + \frac{1}{2K_{\text{Li}\mathbf{1}}\gamma_{\text{Li}}\gamma_{\mathbf{1}}} \frac{\gamma_{\text{Li}\mathbf{1}}}{\gamma_{\mathbf{1}}} - \frac{1}{2} \sqrt{\left(6[\text{Li}_5\mathbf{1}]_{\text{total}} + \frac{1}{K_{\text{Li}\mathbf{1}}\gamma_{\text{Li}}\gamma_{\mathbf{1}}} \frac{\gamma_{\text{Li}\mathbf{1}}}{\gamma_{\mathbf{1}}}\right)^2 - 20[\text{Li}_5\mathbf{1}]_{\text{total}}^2} \quad (27)$$

Finally, combination of eqs 26 and 21 gives an expression for the observed chemical shift (δ) as a function of the total POM concentration ($[\text{Li}_5\mathbf{1}]_{\text{total}}$):

$$\delta = \delta_0 + (\delta_1 - \delta_0) \times \frac{3[\text{Li}_5\mathbf{1}]_{\text{total}} + \frac{1}{2K_{\text{Li}\mathbf{1}}\gamma_{\text{Li}}\gamma_{\mathbf{1}}} \frac{\gamma_{\text{Li}\mathbf{1}}}{\gamma_{\mathbf{1}}} - \frac{1}{2} \sqrt{\left(6[\text{Li}_5\mathbf{1}]_{\text{total}} + \frac{1}{K_{\text{Li}\mathbf{1}}\gamma_{\text{Li}}\gamma_{\mathbf{1}}} \frac{\gamma_{\text{Li}\mathbf{1}}}{\gamma_{\mathbf{1}}}\right)^2 - 20[\text{Li}_5\mathbf{1}]_{\text{total}}^2}}{5[\text{Li}_5\mathbf{1}]_{\text{total}}}$$

A change in the observed chemical shift (δ) as a function of $[\text{Li}_5\mathbf{1}]_{\text{total}}$ was fitted to eq 28 by nonlinear least-squares regression by varying the parameters δ_0 , δ_1 , and $K_{\text{Li}\mathbf{1}}$. The activity coefficient of the Li^+ cation (γ_{Li}) was calculated by using the parameters a and b obtained from nonlinear least-squares fitting of the kinetic data (see Results and Discussion), while the ratio $\gamma_{\text{Li}\mathbf{1}}/\gamma_{\mathbf{1}}$ was approximated as 1.

Results and Discussion

I. Stoichiometry, Rate Law, and Reaction Mechanism. As a prerequisite to rigorous investigation of specific alkali metal cation catalysis of electron transfer, and to reliable correlation of electron-transfer rates with the structure and physical properties of well-defined 1:1 ion pairs, $[(\text{M}^+)(\mathbf{a}\text{-SiVW}_{11}\text{O}_{40}^{5-})]^+$ ($\text{M}^+\mathbf{1}$; $\text{M}^+ = \text{Li}^+, \text{Na}^+, \text{K}^+$), the oxidation of a carefully chosen substrate, 3,3',5,5'-tetra-*tert*-butylphenyl-4,4'-diol (henceforth BPH_2), by $\mathbf{a}\text{-SiV}^{\text{v}}\text{W}_{11}\text{O}_{40}^{5-}$ ($\mathbf{1}$) was studied in detail. The phenolic substrate was selected to provide clean (effectively 100%) conversion to a single oxidation product, in this case, 3,3',5,5'-tetra-*tert*-butyldiphenoquinone (DPQ). The goal of this prerequisite study was to establish the conditions necessary for ensuring highly selective oxidation and well-defined kinetic behavior to high percent conversion values and to determine the mechanism of electron transfer from BPH_2 to $\mathbf{1}$.

Stoichiometry. In 2:3 (v/v) $\text{H}_2\text{O}/t\text{-BuOH}$ at 60 °C, BPH_2 is oxidized by 2 equiv of $\mathbf{1}$ (quantified by UV-vis spectroscopic observation of $\mathbf{1}_{\text{red}}$) to DPQ (eq 1; 100% by ^1H NMR and GC-MS, see Experimental Section).

Orders of Reaction. At constant $[\text{Li}^+]$, the reaction rate is first order in $[\text{BPH}_2]$, first order in $[\mathbf{1}]$, zeroth order in $[\mathbf{1}_{\text{red}}]$ and in $[\text{OAc}^-]$, effectively independent of $[\text{H}^+]$ at pH values smaller than 5, and inversely dependent on $[\text{H}^+]$ at pH values larger than 5.5.

$[\text{BPH}_2]$. The initial rate of formation of $\mathbf{1}_{\text{red}}$ ($d[\mathbf{1}_{\text{red}}]/dt$) was determined by UV-vis spectroscopy. At 60 °C in lithium-acetate-buffered 23 (v/v) $\text{H}_2\text{O}/t\text{-BuOH}$ (100 mM LiOAc and 100 mM HOAc), the rate of reduction of $\mathbf{1}$ (0.4 mM $\text{Li}_5\mathbf{1}$) is first order with respect to $[\text{BPH}_2]$ at BPH_2 concentrations of from 0.3 to ca. 3.6 mM (dashed line in Figure 2a). At BPH_2 concentrations of from 3.0 to 6.0 mM (solid line in Figure 2a), a slightly higher order reaction rate dependence on $[\text{BPH}_2]$ is observed. The higher order dependence observed at high $[\text{BPH}_2]$

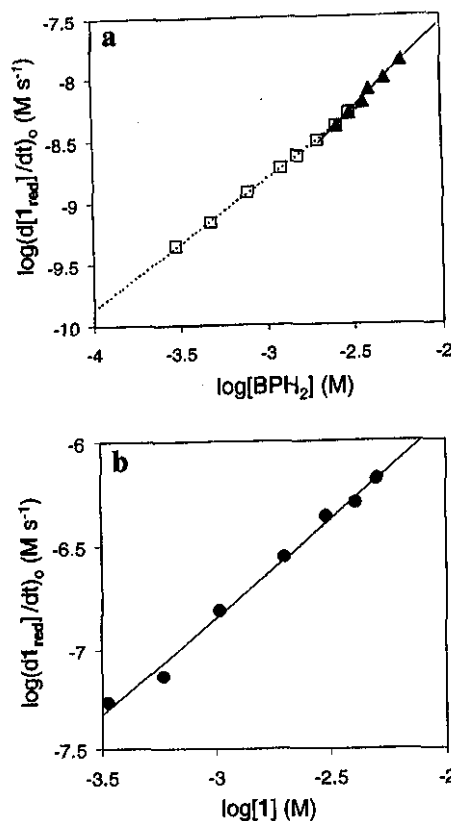


Figure 2. (a) Plot of $\log(\text{initial rate} = d[\mathbf{1}_{\text{red}}]/dt)$ versus $\log [\text{BPH}_2]$; $[\text{BPH}_2] = 0.3\text{--}3.6\text{ mM}$ (dashed line, the slope is 1.06) and $[\text{BPH}_2] = 3.0\text{--}6.0\text{ mM}$ (solid triangles), $[\text{Li}_5\mathbf{1}] = 0.4\text{ mM}$, $[\text{LiOAc}] = 0.1\text{ M}$, $[\text{HOAc}] = 0.1\text{ M}$, 60 °C, (b) Plot of $\log(\text{initial rate} = d[\mathbf{1}_{\text{red}}]/dt)$ versus $\log [\mathbf{1}]$; $[\text{Li}_5\mathbf{1}] = 0.34\text{--}5.0\text{ mM}$, $[\text{BPH}_2] = 6.0\text{ mM}$, $[\text{LiOAc}] = 0.1\text{ M}$, $[\text{HOAc}] = 0.1\text{ M}$, 60 °C.

is attributed to dimerization^{44,45} of BPH_2 in the substantially hydrophilic solvent system needed to solubilize BPH_2 and DPQ.⁴⁶

$[\mathbf{1}]$. At constant $[\text{Li}^+]$ (125 mM), maintained by addition of LiCl (0–23 mM LiCl; ionic strength, μ , varied from 128 to 175 mM)^{47,48} the rate of oxidation of BPH_2 (6.0 mM) is first order with respect to $[\mathbf{1}]$ (0.34–5.0 mM $\text{Li}_5\mathbf{1}$; Figure 2b).⁴⁹

$[\mathbf{1}_{\text{red}}]$. The reaction rate is independent of $[\mathbf{1}_{\text{red}}]$, $[\mathbf{a}\text{-Li}_6\text{SiV}^{\text{v}}\text{W}_{11}\text{O}_{40}]$, over a range of $[\text{Li}_5\mathbf{1}]/[\text{Li}\mathbf{1}]$ ratios varying from 1 to 32. The zeroth-order dependence on $[\mathbf{1}_{\text{red}}]$ was established by varying the concentration of added $\mathbf{1}_{\text{red}}$ from 0.1 to 3.2 mM at constant $[\text{H}^+]$ (Figure S1). (Here, and in all subsequent work, 2.9 mM or smaller concentrations of BPH_2 were used in order to ensure that concentrations of $(\text{BPH}_2)_2$ (see Figure 2a) remained below kinetically significant levels.⁵⁰) The

(44) Tkac, A.; Omelka, L.; Jirackova, L.; Pospisil, J. *Org. Magn. Reson.* **1980**, *14*, 249–255.

(45) Pelikan, P.; Tkac, A.; Omelka, L.; Stasko, A. *Org. Magn. Reson.* **1982**, *20*, 205–211.

(46) Assuming rapid and reversible dimerization in solution ($2\text{BPH}_2 \rightleftharpoons (\text{BPH}_2)_2$), the concentration of $(\text{BPH}_2)_2$ is given by the mass balance relationship $[(\text{BPH}_2)_2] = K_{\text{assoc}}[\text{BPH}_2]^2$, where K_{assoc} is the association constant for dimerization. Provided that the rate of oxidation of $(\text{BPH}_2)_2$ is governed by a bimolecular elementary step (rate = $k_{\text{dimer}}[\mathbf{1}][(\text{BPH}_2)_2]$) analogous to that observed in the oxidation of BPH_2 (i.e., rate = $k[\mathbf{1}][\text{BPH}_2]$; see below), then, by substitution: rate = $k_{\text{dimer}}K_{\text{assoc}}[\mathbf{1}][\text{BPH}_2]^2$. Hence, the overall rate of reduction of $\mathbf{1}$ at the larger $[\text{BPH}_2]$ values (once dimerization becomes kinetically significant) includes contributions from two parallel reactions, one possessing a first-order dependence on $[\text{BPH}_2]$ (oxidation of BPH_2) and the other possessing a second-order dependence on $[\text{BPH}_2]$ (oxidation of $(\text{BPH}_2)_2$). Accordingly, the solid triangles in Figure 2a represent a transitional region between first-order dependence of reaction rate on $[\text{BPH}_2]$ at small $[\text{BPH}_2]$ and second-order dependence at high $[\text{BPH}_2]$ (i.e., at BPH_2 concentrations larger than those studied).

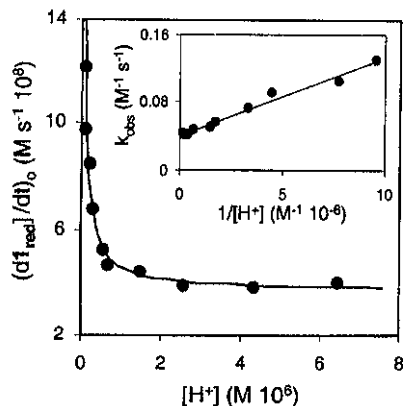


Figure 3. Plot of initial rate = $d[\mathbf{1}_{\text{red}}]/dt$ versus $[\text{H}^+]$; $[\text{H}^+] = 6.5 \times 1.3 \times 10^{-7}$ (pH = 5.19–6.89 measured in acetate-buffered water/*t*-BuOH), $[\text{Li}_2\mathbf{1}] = 0.48$ mM, $[\text{BPH}_2] = 2.86$ mM, $[\text{LiOAc}] = 0.1$ M, 60 °C. Inset: Plot of k_{obs} versus $1/[\text{H}^+]$.

lack of a decrease in rate upon addition of $\mathbf{1}_{\text{red}}$ shows that reduction of $\mathbf{1}$ to $\mathbf{1}_{\text{red}}$ in the rate-limiting elementary step (e.g., reduction of $\mathbf{1}$ to $\mathbf{1}_{\text{red}}$ within the $[\text{BPH}_2, \mathbf{1}]^{\text{S-}}$ donor–acceptor pair) is irreversible. Reactions responsible for irreversible reduction of $\mathbf{1}$ might include rapid loss of H^+ from the successor complex, $[\text{BPH}_2^{\bullet}, \mathbf{1}_{\text{red}}]^{\text{S-}}$, to give $[\text{BPH}^{\bullet}, \mathbf{1}_{\text{red}}]^{\text{S-}}$.

[OAc]. Rapid loss of H^+ from $[\text{BPH}_2^{\bullet}, \mathbf{1}_{\text{red}}]^{\text{S-}}$ (or from BPH_2^{\bullet}) is suggested by the absence of general base catalysis. Initial rate ($d[\mathbf{1}_{\text{red}}]/dt$) values remain effectively unchanged as the concentration of LiOAc (along with equimolar concentrations of HOAc) is increased from 10 to 200 mM at constant $[\text{H}^+]$, $[\text{Li}^+]$, and ionic strength (Figure S2).

[H⁺]. The dependence of reaction rate on $[\text{H}^+]$ was investigated over a pH range of from 5.19 to 6.89 (6.5×10^{-6} – 1.3×10^{-7} M H^+ ; Figure 3). pH values were systematically increased by decreasing the concentration of HOAc at constant (0.1 M) $[\text{LiOAc}]$ (in these experiments, pH values of acetate-buffered $\text{H}_2\text{O}/t\text{-BuOH}$ solutions were measured directly; see Experimental Section). Acid dissociation of BPH_2 to BPH^- becomes kinetically significant at pH values above ca. 5.5 (i.e., at $[\text{H}^+]$ values smaller than 3.15×10^{-6} M). A linear plot of k_{obs} values versus

(47) The reaction rate at constant $[\text{Li}^+]$ is insensitive to modest changes in ionic strength (see Table 2, below). Moreover, as shown in detail below (Results and Discussion, part II), ion pairing between Li^+ and $\mathbf{1}$ has a far greater effect on reaction rates than do comparable changes in ionic strength alone. Molal-scale μ values are approximated here by molar-scale values calculated by using molar values in place of molal, m , values in the Debye–Hückel relationship, $0.5\Sigma z^2m$. The Debye–Hückel relationship itself, although derived for dilute solutions of low-valent (ideally 1:1) electrolytes, has been successfully applied to theoretical calculations of rates of outer-sphere electron self-exchange between Keggin anions possessing charges of 3–, 4–, and 5– (ref 48).

(48) Kozik, M.; Baker, L. C. W. *J. Am. Chem. Soc.* **1990**, *112*, 7604–7611.

(49) The observation of a first-order dependence of initial reaction rate on $[\mathbf{1}]$ at 6.0 mM BPH_2 (i.e., corresponding to the solid triangle in Figure 2a associated with a $\log [\text{BPH}_2]$ value of -2.2 on the abscissa) demonstrates first-order dependence on $[\mathbf{1}]$ for each of the two simultaneous reactions, the oxidations of BPH_2 and of $(\text{BPH}_2)_2$. The 6.0 mM BPH_2 concentration was used for convenience to more rapidly obtain the initial rate data shown in Figure 2b. However, the first-order dependence on $[\mathbf{1}]$ at 2.0 mM BPH_2 , wherein the concentration of $(\text{BPH}_2)_2$ was not kinetically significant, was unambiguously established to over 90% conversion by nonlinear least-squares regression analysis of absorbance versus time data (see Figure 5 below) for the reaction of $\mathbf{1}$ (1.0 mM) with BPH_2 , fitted to an explicit expression derived by using the bimolecular rate law, $(d[\mathbf{1}_{\text{red}}]/dt) = k_{\text{obs}}[\mathbf{1}][\text{BPH}_2]$ (eq 29; constant $[\text{H}^+]$).

(50) Using 1.0 mM $\text{Li}_2\mathbf{1}$ and 100 mM LiOAc, $[\text{Li}^+]$ increased slightly from 106 mM at 0.1 mM $\text{Li}_2\mathbf{1}_{\text{red}}$ to 124 mM at 3.2 mM $\text{Li}_2\mathbf{1}_{\text{red}}$. This variation in $[\text{Li}^+]$ (at relatively high $[\text{Li}^+]$, i.e., at $[\text{Li}^+]$ values over ca. 100 mM), and the associated increase in ionic strength, are not kinetically significant (see Table 2 and Figure 7, below.)

$1/[\text{H}^+]$ at pH values larger than ca. 5.5 (Figure 3, inset; $k_{\text{obs}} = (d[\mathbf{1}_{\text{red}}]/dt)/([\text{Li}_2\mathbf{1}][\text{BPH}_2])$) reveals an inverse dependence on $[\text{H}^+]$. The dependence of rate on $[\text{H}^+]$ approaches zero at high $[\text{H}^+]$ (see eq 36, below).

Rate Law. The data presented here (Figures 2, 3, S1, and S2) show that at constant $[\text{Li}^+]$, and at $[\text{BPH}_2]$ values smaller than 3 mM, the reaction rate is first order in $[\mathbf{1}]$, first order in $[\text{BPH}_2]$, zeroth order in $[\mathbf{1}_{\text{red}}]$, zeroth order in $[\text{OAc}^-]$, and zeroth order in $[\text{H}^+]$ at pH values smaller than 5, and asymptotically approaches inverse first order in $[\text{H}^+]$ as pH values increase above 5.5. Using UV–vis to measure the rate of formation of $\mathbf{1}_{\text{red}}$, taking into account the 2:1 $\mathbf{1}:\text{BPH}_2$ stoichiometry shown in eq 1, and defining the reaction rate as $d[\text{DPQ}]/dt = 1/2(d[\mathbf{1}_{\text{red}}]/dt)$, the empirical rate law for reaction of $\mathbf{1}$ with BPH_2 at pH values smaller than 5 is given by eq 29.

$$\frac{1}{2} \frac{d[\mathbf{1}_{\text{red}}]}{dt} = k_{\text{obs}}[\mathbf{1}]^1[\text{BPH}_2]^1[\text{OAc}^-]^0[\mathbf{1}_{\text{red}}]^0[\text{H}^+]^0 \quad (29)$$

Preassociation. Combined ^1H and ^{51}V NMR analysis of solutions of BPH_2 and $\mathbf{1}$ in acetate-buffered 2:3 (v/v) $\text{D}_2\text{O}/t\text{-BuOH}$ provided no evidence for the formation of stable association complexes, 25,51 $[(\text{BPH}_2)(\mathbf{1})]$, prior to electron transfer. The NMR study was carried out at room temperature (at which the rate of reduction of $\mathbf{1}$ by BPH_2 is small) using a range of absolute and relative concentrations of both BPH_2 and $\mathbf{1}$. Prior to addition of *t*-BuOH, the pD of each D_2O solutions was adjusted to 4.76 (using LiOAc and DOAc) to ensure that the concentration of BPH^- was kinetically insignificant. No changes in ^1H or ^{51}V NMR that might plausibly be attributed to association were observed. Moreover, the relatively large negative entropy of activation, DS^\ddagger , associated with the reaction (-39 ± 5 cal $\text{mol}^{-1} \text{K}^{-1}$; see temperature dependence data immediately below) is consistent with a bimolecular rate-limiting step.

Activation Parameters. The temperature dependence of k_{obs} was determined at pH 4.76 (aqueous phase prior to addition of *t*-BuOH) to ensure that only BPH_2 (not dissociated to BPH^- and H^+) was present at a kinetically significant concentration. Activation parameters of $\text{DH}^\ddagger = 8.5 \pm 1.4$ kcal mol^{-1} and $\text{DS}^\ddagger = -39 \pm 5$ cal $\text{mol}^{-1} \text{K}^{-1}$ were calculated from a plot of $\ln(k_{\text{obs}}/T)$ versus $1/T$ (Figure S3, five measurements from 323 to 358 K, $R^2 = 0.98$). The low DH^\ddagger is consistent with outer-sphere electron transfer. The relatively large DS^\ddagger value likely includes contributions from a sterically and orientationally restricted activated complex. A steric constraint is associated with the presence of bulky *tert*-butyl groups on either side of the phenolic hydroxyl moiety in BPH_2 . 32a The orientational restraint 52 arises from the very low ratio of the surface areas of the reactive C–OH and V=O moieties to the total surface areas of BPH_2 and $\mathbf{1}$ (ca. 0.02 and 0.004, respectively). The large negative entropy of activation might thus be due, in part, to a requirement that the BPH_2 and POM molecules are rotated such that their respective donor (C–OH) and acceptor (V=O) sites are adjacent to one another prior to electron transfer.

Ionic Strength. The dependence of reaction rate on ionic strength was determined by using 2.0 mM solutions of BPH_2 at pH 4.76 (aqueous solution prior to addition of *t*-BuOH). Due to ion pairing, the reaction rate is sensitive to $[\text{Li}^+]$. It was therefore necessary to vary ionic strength values without changing the total Li^+ concentration. To accomplish this, the

(51) Neumann, R.; Levin, M. *J. Am. Chem. Soc.* **1992**, *114*, 7278–7286.

(52) Wang, Y.; Cardona, C. M.; Kaifer, A. E. *J. Am. Chem. Soc.* **1999**, *121*, 9756–9757.

Table 2. Dependence of k_{obs} Values on Ionic Strength (μ) at Constant Total Alkali Metal Cation (Li^+) Concentration^a

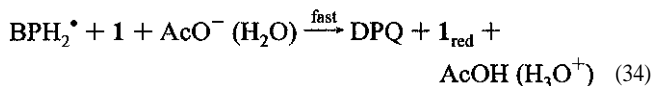
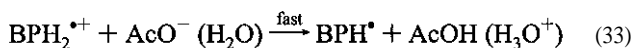
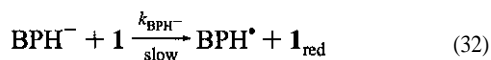
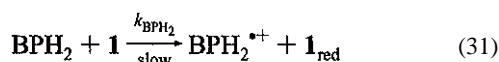
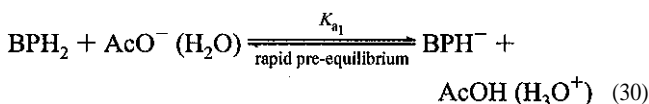
[LiCl] (mM)	[Li ₆ 2] (mM)	[Li ⁺] ^b (mM)	μ^c (mM)	$E_{1/2}^d$ (V)	k_{obs} ($\times 10^{-2} \text{ M}^{-1} \text{ s}^{-1}$)
10.2		13.1	16.9	0.248	1.99 ± 0.13
	1.60	12.5	40.4	0.231	1.61 ± 0.10

^a [BPH₂] = 2.00 mM, [Li₃1] = 1.00 mM, in 1.0 mM LiOAc/HOAc-buffered water/*t*-BuOH solution (2:3 v/v), pH 4.16, 60 °C, under Ar.

^b $[\text{Li}^+] = [\text{LiCl}] + 6[\text{Li}_6\mathbf{2}] + 5[\text{Li}_3\mathbf{1}] + [\text{LiOAc}]$. ^c $\mu = (2[\text{LiCl}] + 42[\text{Li}_6\mathbf{2}] + 30[\text{Li}_3\mathbf{1}] + 2[\text{LiOAc}])/2$. ^d $E_{1/2} = (E_c + E_a)/2$ versus Ag/AgCl reference electrode.

anions were varied by using LiCl or Li₆Al(OiOH₂)W₁₁O₃₉ (Li₆2)⁵⁴ as the electrolyte (Table 2). An approximate doubling of the ionic strength from 16.9 (10 mM LiCl added) to 40.4 mM (1.60 mM Li₆2 added) had little effect on k_{obs} . Study over a larger range of ionic strength values, while desirable, was prohibited by limitations in the solubility of Li₆2. In addition, uncertainty regarding the degree of ion pairing between Li⁺ and Cl⁻ and between Li⁺ and 2 makes it difficult to precisely assign ionic strength values. Nonetheless, the absence of an increase in k_{obs} at the larger ionic strength value is consistent with a rate-limiting bimolecular step involving at least one neutral reactant (i.e., BPH₂).⁵³ Although rate-limiting reaction between BPH• and 1 would also be consistent with the effective absence of an ionic strength dependence, the inverse dependence on [H⁺] points to rate-limiting oxidation of BPH₂ (and of its conjugate base, BPH⁻). In addition, the absence of a kinetic deuterium isotope effect in the oxidation of nondissociated BPH₂ (at pH (pD) values below ca. 5; see these data below) argues against rate-limiting proton-coupled electron-transfer oxidation of BPH⁻ to DPQ. An unfavorable change in $\text{DG}^\circ_{\text{et}}$ associated with formation of the highly energetic cation BPH₂•⁺ (i.e., ca. $-RT \ln K_a$, where K_a is the acid dissociation constant of BPH₂•⁺)^{54,55} is offset by electrostatically favorable interaction between BPH₂•⁺ and 1_{red} in the successor complex [(BPH₂•⁺), (SiV^{IV}W₁₁O₄₀•⁶⁻)]⁵⁻.

Reaction Mechanism. The reaction sequence in eqs 30–34 for reaction of BPH₂ with 1 at constant [Li⁺] is consistent with all the data reported above.



Application of a steady-state approximation to the intermediates in eqs 30–34 ($d[\text{BPH}_2^\bullet]/dt = d[\text{BPH}^\bullet]/dt = 0$) gives the following derived expression:

$$\frac{1}{2} \frac{d[\mathbf{1}_{\text{red}}]}{dt} = \left(\frac{k_{\text{BPH}_2}[\text{H}^+] + k_{\text{BPH}}K_{a1}}{K_{a1} + [\text{H}^+]} \right) [\mathbf{1}][\text{BPH}_2] \quad (35)$$

where k_{BPH_2} and k_{BPH} are rate constants for reaction of 1,

respectively, with BPH₂ and with monoanionic BPH⁻, and K_{a1} is the first acid dissociation constant of BPH₂. Using the fact that $K_{a1} \ll [\text{H}^+]$ (values of K_{a1} are estimated on the basis of literature values to be ca. 10^{-14} – 10^{-15} M,^{56–59} while experimental [H⁺] values ranged from ca. 10^{-6} to 10^{-7} M), eq 35 simplifies to eq 36.

$$\frac{1}{2} \frac{d[\mathbf{1}_{\text{red}}]}{dt} = \left(k_{\text{BPH}_2} + \frac{k_{\text{BPH}}K_{a1}}{[\text{H}^+]} \right) [\mathbf{1}][\text{BPH}_2] \quad (36)$$

This expression reflects the inverse dependence of k_{obs} on [H⁺] (Figure 3, inset) and is identical to a more general form of the empirical rate law (eq 29), in which $k_{\text{obs}} = k_{\text{BPH}_2} + (k_{\text{BPH}}K_{a1})/[\text{H}^+]$.

Independent support for eq 36 (and, by implication, eqs 30–34) is provided by comparison of the experimental $k_{\text{BPH}}/k_{\text{BPH}_2}$ ratio to literature values for related phenols. The product of k_{BPH} and K_{a1} is obtained directly from the slope of the plot of k_{obs} versus $1/[\text{H}^+]$ (inset in Figure 3), while k_{BPH_2} (high [H⁺] limit; *y*-intercept in the Figure 3 inset) is $0.02 \text{ M}^{-1} \text{ s}^{-1}$. An estimated value of $K_{a1} = 10^{-14}$ – 10^{-15} M for BPH₂ in 2:3 (v/v) H₂O/*t*-BuOH at 60 °C was calculated by extrapolation of K_a values reported for closely related phenols in water/alcohol mixtures at several temperatures (see Tables S1 and S2).^{56–59} The estimated K_{a1} value (10^{-14} – 10^{-15} M) gives $k_{\text{BPH}} \gg 10^6$ – $10^7 \text{ M}^{-1} \text{ s}^{-1}$. Thus, the reactivity of the BPH⁻ monoanion toward 1 is roughly 10^7 – 10^8 times that of BPH₂ (i.e., $k_{\text{BPH}}/k_{\text{BPH}_2} = 10^7$ – 10^8). This value is consistent with reported $k_{\text{phenolate}}/k_{\text{phenol}}$ ratios.^{60–62}

Kinetic Deuterium Isotope Effect. Kinetic deuterium isotope data ($k_{\text{H}}/k_{\text{D}}$ for oxidation of BPH₂ versus that of BPD₂) provide no indication of bond breaking in the rate-limiting elementary step (eq 31) but, rather, reflect a difference in acid dissociation constants of BPH₂ and BPD₂ (eq 30). Comparison of initial reaction rate data obtained by using BPH₂ in H₂O/*t*-BuOH with those obtained by using BPD₂ in deuterated solvent (D₂O and *tert*-butyl alcohol-*d*) gives a $k_{\text{H}}/k_{\text{D}}$ value of 2.0 ± 0.3 at pH

(53) The slight decrease in k_{obs} observed upon an increase in ionic strength is attributed to a small decrease in the reduction potential upon changing the electrolyte from LiCl to Li₆2. $E_{1/2}$ values of the two solutions of 1 are included in Table 2; correlation between k_{obs} and $E_{1/2}$ values is elaborated in the Discussion section, below. As is shown there, an increase in $E_{1/2}$ implies a greater degree of association between Li⁺ and 1. This increased association is reflected in larger k_{obs} values. At low [Li⁺] values, i.e., ca. 6–25 mM [Li⁺], $E_{1/2}$ and k_{obs} values are both highly sensitive to small changes in the activities of Li⁺. The actual activities of Li⁺, which apparently differ slightly despite efforts to keep total Li⁺ concentrations identical, depend on several factors, including the relative extents of electrolyte (LiCl or Li₆2) self-association. Thus, at nearly identical total Li⁺ concentrations, slightly greater association between Li⁺ and 2 (relative to that between Li⁺ and Cl⁻) would lead to a smaller activity for Li⁺ in the Li₆2 solution and, hence, to a slightly lower k_{obs} value.

(54) Thompson, M. S.; Meyer, T. J. *J. Am. Chem. Soc.* **1982**, *104*, 5070–5076.

(55) Thompson, M. S.; Meyer, T. J. *J. Am. Chem. Soc.* **1982**, *104*, 4106–4115.

(56) England, B. D.; House, D. A. *J. Chem. Soc.* **1962**, 4421–4423.

(57) Cohen, L. A.; Jones, W. M. *J. Am. Chem. Soc.* **1963**, *85*, 3397–3402.

(58) *Dictionary of Organic Compounds*, 6th ed.; Chapman & Hall: London, 1996; Vol. 1.

(59) Mohanty, J.; Pal, H.; Sapre, A. V. *Bull. Chem. Soc. Jpn.* **1999**, *72*, 2193–2202.

(60) Tee, O. S.; Paventi, M.; Bennett, J. M. *J. Am. Chem. Soc.* **1989**, *111*, 2233–2240.

(61) Wajon, J. E.; Rosenblatt, D. H.; Burrows, E. P. *Environ. Sci. Technol.* **1982**, *16*, 396–402.

(62) Grimley, E.; Gordon, G. *J. Inorg. Nucl. Chem.* **1973**, *35*, 2283–2392.

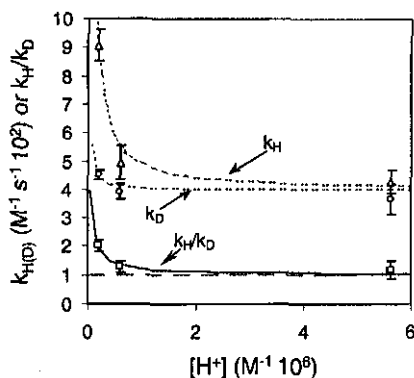


Figure 4. Plot of observed rate constants (k_H and k_D ; triangles and circles, respectively) and k_H/k_D ratios (squares) versus $[H^+]$, and best fits to eq 36 (and its equivalent for reaction in deuterated solvent) for k_H and k_D values (dashed lines). The ratio (k_H/k_D) of calculated k_H and k_D values is shown by a solid line.

5.45 and pD 5.44. At pH 3.90 and pD 3.90 (measured in H₂O or D₂O prior to mixing with *t*-BuOH), however, a k_H/k_D value of 1.2 ± 0.2 is observed.

These data reflect the greater acidity of BPH₂ in protiated solvent relative to that of BPD₂ in deuterated solvent.⁶³ Because BPD₂ is a weaker acid (i.e., it possesses a larger pK_{a1} value), the steady-state concentration of BPD⁻ remains smaller and kinetically less important at pD (pH) values at which dissociation of BPH₂ becomes kinetically significant (k_H and k_D values are plotted at the top of Figure 4; the fitted curves were calculated by using eq 36).⁶⁴ At lower pD (pH) values, however, concentrations of BPD⁻ and BPH⁻ are both very small, and initial rate data converge to a common k_{obs} value associated with undissociated BPD₂ and BPH₂ (convergence of k_H/k_D ratios as pH (pD) values decrease is shown at the bottom of Figure 4). Thus, successful fitting of k_H and k_D values calculated by using eq 36 and convergence of k_H/k_D ratios at lower pH (pD) values fully account for the difference in rates observed for oxidations of BPH₂ and BPD₂. Moreover, convergence of k_H/k_D ratios as pH (pD) values decrease indicates that cleavage of the phenolic O–H bond in BPH₂ (H⁺-coupled electron transfer, H⁺ or H⁻ transfer) is not kinetically significant. These data thus provide additional support for a mechanism involving rate-limiting electron transfer from BPH₂ to **1** (i.e., in eqs 30–34).

Applicability of Rate Law to High Percent Conversion Values. The results reported in Figures 2–4 (and in Figures S1–S3) were obtained by use of initial rate data. However, it is often the case that reaction pathways unimportant during the initial phase of a reaction can become kinetically significant at high conversion after reactant concentrations have decreased well below their initial values. Nonlinear least-squares regression analysis of absorbance versus time data was used to provide further support for eq 29 (at constant $[H^+]$, such that eq 29 reduces to rate = $k_{obs}[1][BPH_2]$), and to confirm that the reaction obeys this relationship to high (90–95%) conversion of BPH₂ to DPQ. An explicit expression was derived for the reaction and stoichiometry in eq 1 by integration of the effectively

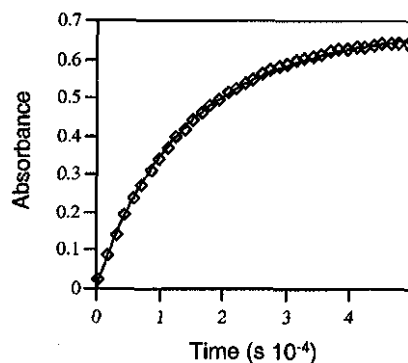


Figure 5. Absorbance at 520 nm (I_{obs}) versus time data (open diamonds; for clarity, every other point is plotted) for the oxidation of BPH₂ by Li₂I and nonlinear least-squares fit of eq 37 (solid line; $k_{obs} = 2.02 \times 10^{-2} M^{-1} s^{-1}$, sum of standardized square residuals = 2.9×10^{-3} . Reaction conditions: $[I] = 1.1$ mM, $[BPH_2] = 1.9$ mM, $[LiOAc] = 1$ mM, $[HOAc] = 1$ mM, $[LiCl] = 10.2$ mM, 23 (v/v) H₂O/*t*-BuOH, under Ar at 60 °C.

second-order rate law in eq 29 (see derivation of eq 37 in Experimental Section):

$$A_t = \epsilon \left\{ [1]_0 - \frac{[BPH_2]_0 - \frac{[1]_0}{2}}{[1]_0} \exp \left[k_{obs} \left([BPH_2]_0 - \frac{[1]_0}{2} \right) t \right] - \frac{1}{2} \right\} + A_0 \quad (37)$$

Nonlinear regression was then used to fit absorbance versus time data to eq 37. The sum of standardized square residuals was minimized by varying the value of k_{obs} . The reaction was carried out under well-behaved conditions—pH 4.76 and $[BPH_2]$ less than 3.0 mM so that $[BPH^-]$ and $[(BPH_2)_2]$ were both below kinetically significant levels—and followed to over 90% completion. Excellent fit between experimental and calculated values (Figure 5) provides additional support for eqs 29 and 36 and demonstrates that the reaction is well behaved to high percent conversion values. Moreover, the k_{obs} value (one-half of k_{obs} in eq 3) obtained by nonlinear regression analysis ($2.02 \pm 0.05 \times 10^{-2} M^{-1} s^{-1}$) closely matches that obtained by use of initial rate methods and eq 29 under the same reaction conditions ($2.10 \pm 0.08 \times 10^{-2} M^{-1} s^{-1}$).

II. Electron Transfer to Solvent-Separated 1:1 Ion Pairs, [(M⁺)(SiVW₁₁O₄₀⁵⁻)]⁺ (M⁺ = Li⁺, Na⁺, K⁺). The data presented above establish the reaction conditions and concentrations necessary for the selective oxidation of BPH₂ (monomeric and not dissociated into BPH⁻ and H⁺) to DPQ by kinetically well defined outer-sphere electron transfer to **1**. The extensive efforts needed to obtain this information were undertaken so that further kinetic data could be used reliably to establish the 1:1 stoichiometry of formation of the ion pairs, [(M⁺)(SiVW₁₁O₄₀⁵⁻)]⁺ (M⁺**1**, M⁺ = Li⁺, Na⁺, K⁺), to determine associated formation constants, and to investigate in detail the fundamental role of alkali metal cation size on ion pair structure and on the energy and rate of electron transfer from BPH₂ to M⁺**1** pairs.

Reaction Conditions and Rate Law. To avoid dimerization of BPH₂ to (BPH₂)₂, the experiments described in this section were carried out by using BPH₂ concentrations below 3.0 mM; concentrations of anionic BPH⁻ were limited to kinetically insignificant levels by using alkali metal acetate MOAc/HOAc buffers to maintain solution pH values at 4.76. Under these conditions, reaction rates obey eq 38, rate = $k_{obs}[1][BPH_2]$, with k_{obs} from eq 36 equal to a single term, k_{BPH_2} , i.e., the $[H^+]$ -

(63) Lowry, T. H.; Richardson, K. S. *Mechanism and Theory in Organic Chemistry*, 3rd ed.; Harper & Row Publishers: New York, 1987.

(64) The k_H curve was generated by fitting data from initial rate measurements obtained at 10 pH values (only three of these are shown in Figure 4; the others are shown in Figure 3) to eq 36 by varying two parameters, k_{BPH_2} and $k_{BPH^-}K_{a1}$. This curve is functionally equivalent to that in Figure 3 (rate versus $[H^+]$). The k_D curve was generated by fitting data from initial rate measurements obtained at three pD values to a function identical in form to eq 36 by varying k_{BPH_2} and $k_{BPH^-}K_{a1}$.

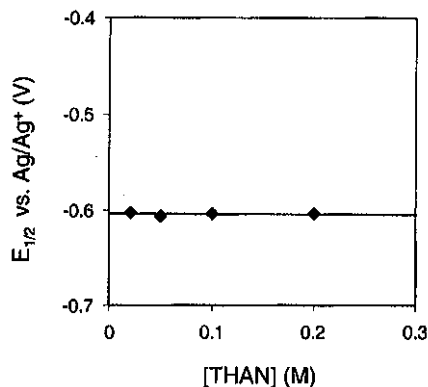


Figure 6. Potential, $E_{1/2}$, of the $1/1_{\text{red}}$ couple (1.0 mM $\text{THA}_5\mathbf{1}$) in 2:3 (v/v) $\text{H}_2\text{O}/t\text{-BuOH}$ at 60 °C in the presence of 25–200 mM tetra-*n*-hexylammonium nitrate (THAN) electrolyte. $E_{1/2}$ values are referenced to Ag/AgNO_3 (see Experimental Section).

dependent term in eq 36 is small.

$$\frac{1}{2} \frac{d[1_{\text{red}}]}{dt} = k_{\text{BPH}_2}[1][\text{BPH}_2] \quad (38)$$

Electron Transfer in the Absence of Ion Pairing. A baseline value for k_{BPH_2} in the absence of ion pairing was obtained by use of an effectively nonassociating quaternary alkylammonium cation (R_4N^+) as counterion to $\mathbf{1}$. An appropriate counterion was chosen from among the series $\text{R} = \text{ethyl}, n\text{-propyl}, n\text{-butyl}, n\text{-pentyl}, n\text{-hexyl}$. Unlike the Li^+ , Na^+ , and K^+ salts of $\mathbf{1}$, most of the tetraalkylammonium salts of $\mathbf{1}$ and 1_{red} possess very low solubilities in 2:3 (v/v) $\text{H}_2\text{O}/t\text{-BuOH}$, even at 60 °C. Of the alkylammonium ions listed here, tetra-*n*-hexylammonium was exceptional in that homogeneous solutions of (*n*-hexyl $_4\text{N}^+$) $_5\mathbf{1}$ ($\text{THA}_5\mathbf{1}$) (obtained from $\text{Li}_5\mathbf{1}$ by cation exchange) could be prepared. It was hoped that *n*-hexyl $_4\text{N}^+$ is sufficiently large and hydrophobic that it, effectively, would not form ion pairs with $\mathbf{1}$ in the low dielectric and substantially hydrophobic solvent system (the dielectric constant of 2:3 (v/v) $\text{H}_2\text{O}/t\text{-BuOH}$ at 60 °C is estimated from literature data to be 23.9).⁶⁵ If present, ion pairing between *n*-hexyl $_4\text{N}^+$ and $\mathbf{1}$ or 1_{red} would result in a positive shift in the potential of the $1/1_{\text{red}}$ couple upon increase in the concentration of *n*-hexyl $_4\text{N}^+$ -salt electrolyte.³⁹ However, no increase or decrease in $E_{1/2}$ values of solutions of $\mathbf{1}$ (1 mM) were observed when concentrations of *n*-hexyl $_4\text{N}^+\text{NO}_3^-$ (tetra-*n*-hexylammonium nitrate, THAN) were varied from 25 to 200 mM (Figure 6).⁶⁶

Next, initial rate methods were used to measure k_{BPH_2} for reaction of $\text{THA}_5\mathbf{1}$ with BPH_2 . The reactions were carried out by using 0.5 mM $\text{THA}_5\mathbf{1}$ and 2.0 mM BPH_2 in 2:3 (v/v) $\text{H}_2\text{O}/t\text{-BuOH}$ at 60 °C. Prior to addition of *t*-BuOH, the water used to prepare the solvent system was acidified to a pH of 4.76 by addition of tetra-*n*-hexylammonium hydroxide and acetic acid (THAOH and HOAc ; 1 mM OAc^-). Initial rate data were also used to calculate k_{obs} values after addition of 50 and 100 mM THAN. The k_{obs} value obtained in the absence of added THAN is the rate constant for oxidation of BPH_2 (k_{BPH_2} in eq 38) by effectively unpaired $\mathbf{1}$. Consistent with minimum pairing between THA and $\mathbf{1}$, effectively identical k_{obs} values (within experimental error) are observed after additions of 100 and 200 mM THAN (Figure 7).

(65) Akerlöf, G. *J. Am. Chem. Soc.* **1932**, *54*, 4125–4139.

(66) The Ag/Ag^+ reference electrode used contained 0.01 M AgNO_3 and 0.1 M THAN in 2:3 (v/v) $\text{H}_2\text{O}/t\text{-BuOH}$. In this cell, acceptable results (at least quasi-reversible electrode kinetics and relatively small liquid–liquid junction potentials) required electrolyte concentrations of at least 25 mM.

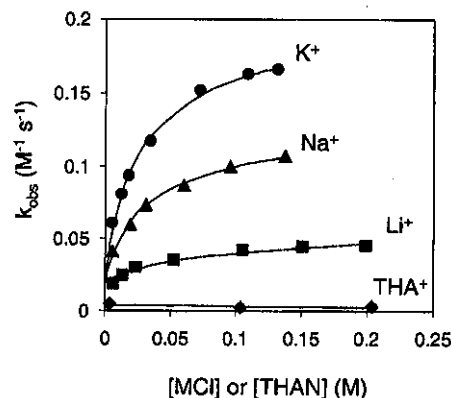
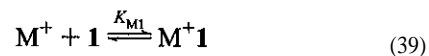


Figure 7. Plot of initial rate ($d[1_{\text{red}}]/dt$) in the presence of 0, 100, and 200 mM THAN, $[\text{THAOAc}] = [\text{HOAc}] = 1$ mM, $[\text{THA}_5\mathbf{1}] = 0.5$ mM, and of initial rate versus $[\text{M}^+]$ ($\text{M}^+ = \text{Li}^+, \text{Na}^+$ and K^+); $[\text{M}^+] = [\text{MCl}] + 5[\text{M}_5\mathbf{1}] + [\text{MOAc}]$, $[\text{MCl}] = 0.0\text{--}0.2$ M, $[\text{M}_5\mathbf{1}] = 1.0$ mM, $[\text{MOAc}] = [\text{HOAc}] = 1$ mM (2.0 mM BPH_2 in 2:3 (v/v) $\text{H}_2\text{O}/t\text{-BuOH}$ at 60 °C).

Observed Dependence of Reaction Rate on $[\text{M}^+]$ ($\text{M}^+ = \text{Li}^+, \text{Na}^+, \text{K}^+$). Initial rate data were then obtained for reactions of $\text{Li}_5\mathbf{1}$, $\text{Na}_5\mathbf{1}$, and $\text{K}_5\mathbf{1}$ as a function of added $[\text{MCl}]$ ($\text{M}^+ = \text{Li}^+, \text{Na}^+, \text{K}^+$, along with buffers prepared by using LiOAc , NaOAc , and KOAc , respectively); 20 k_{obs} measurements in all. For each alkali metal cation, M^+ (Li^+, Na^+ , or K^+), k_{obs} values increase with an increase in $[\text{M}^+]$ (Figure 7). Because k_{obs} values are insensitive to changes in ionic strength (Table 2 and plot of initial rate versus $[\text{THAN}]$ in Figure 7), changes in k_{obs} values as a function of $[\text{M}^+]$ are associated with ion pair formation between M^+ and the 5- anion, $\mathbf{1}$. The challenge presented by these data, however, is to differentiate between contributions to the ordering in k_{obs} values ($\text{Li}^+ < \text{Na}^+ < \text{K}^+$) attributable to ion pair stoichiometries, to K_{IP} values, and to the structures and electronic properties of specific ion pairs.

Specific Functional Dependence of k_{obs} on $[\text{M}^+]$. At infinite dilution, dissolved POM salts exist as fully dissociated counterions, M^+ , and POM anions. At finite $[\text{M}^+]$ values, ion pairing occurs. On the basis of electrostatic arguments^{67–69} and numerous documented reports,^{39,70–72} ion pairing occurs sequentially, with K_{IP} for formation of the 1:1 pair in eq 39 (K_{M1}) larger than K_{IP} values for the formation of higher order, i.e., 2:1, 3:1, etc., ion pairs.



where the equilibrium concentration of $\text{M}^+\mathbf{1}$ is given by the mass balance expression, $K_{\text{M1}} = [\text{M}^+\mathbf{1}]/([\text{M}^+][\mathbf{1}])$. Expansion of eq 38 to include rate constants associated with unpaired $\mathbf{1}$ (k_1) and with 1:1 $\text{M}^+\mathbf{1}$ pairs (k_{M1}) gives

$$\frac{1}{2} \frac{d[1_{\text{red}}]}{dt} = k_1[1][\text{BPH}_2] + k_{\text{M1}}[\text{M}^+\mathbf{1}][\text{BPH}_2] \quad (40)$$

Use of $K_{\text{M1}}[\text{M}^+][\mathbf{1}] = [\text{M}^+\mathbf{1}]$ and rearranging (see Experimental Section) gives

- (67) Fuoss, R. M. *J. Am. Chem. Soc.* **1957**, *79*, 3301–3303.
 (68) Fuoss, R. M.; Kraus, C. A. *J. Am. Chem. Soc.* **1957**, *79*, 3304–3310.
 (69) Fuoss, R. M. *J. Am. Chem. Soc.* **1958**, *80*, 5059–5061.
 (70) Lindmark, A. F. *Inorg. Chem.* **1992**, *31*, 3507–3513.
 (71) Andreu, R.; Calvente, J. J.; Fawcett, W. R.; Molero, M. *J. Phys. Chem.* **1997**, *101*, 2884–2894.
 (72) Capewell, S. G.; Hefter, G. T.; May, P. M. *Talanta* **1999**, *49*, 25–30.

$$\frac{1}{2} \frac{d[\mathbf{1}_{\text{red}}]}{dt} = \left(\frac{k_1 + k_{M1} K_{M1} [M^+] \gamma_M}{1 + K_{M1} [M^+] \gamma_M} \right) [\mathbf{1}] [\text{BPH}_2] \quad (41)$$

The complex rate constant in eq 41 is a rectangular hyperbolic function equal to k_1 at the low $[M^+]$ limit, and which asymptotically approaches k_{M1} as $[M^+]$ increases to large values.^{73,74}

The solid curves in Figure 7 were calculated by simultaneous nonlinear least-squares fitting of all the alkali metal cation data (20 k_{obs} values) to the complex rate constant in eq 41, with the stipulation that all three curves converge to a single k_1 value. Convergence to a single k_{obs} value (k_1) at infinite dilution is implicit to derivation of eq 41. At the same time, the three curves (one for each of the cations, Li⁺, Na⁺ and K⁺) each provide unique values for k_{M1} and K_{M1} , i.e., k_{Li1} , k_{Na1} , k_{K1} , K_{Li1} , K_{Na1} , and K_{K1} .

The rate constant in eq 41 is formally a function of activities of all species present. However, the changes in activities of **1** and BPH₂, whose initial concentrations are small and constant in all experiments, are much less significant than changes in the activities of the alkali metal cations, whose concentrations vary from 5 to over 200 mM (concentrations based on grams of salts MCl present per liter of solution). To minimize the number of adjustable parameters so that meaningful k_1 , k_{M1} , and K_{M1} values could be calculated by nonlinear least-squares regression of the kinetic data, the single most significant activity coefficient, γ_M (for M⁺), was retained.^{39,40,75}

Ion Pair Stoichiometry. Three lines of evidence establish the stoichiometry in eq 39: (1) agreement between k_{obs} values and the complex rate constant in eq 41 over a statistically meaningful range of $[M^+]$ values,⁷⁶ (2) convergence of all three curves (for Li⁺, Na⁺, and K⁺) to a single low $[M^+]$ limit k_1 value; and (3) near identity⁷⁷ between the calculated k_1 value and the k_{obs} value determined by using THA₅L.

Calculation of K_{M1} and k_{M1} . Having established the stoichiometry in eq 39, nonlinear least-squares fitting of the alkali metal cation data in Figure 7 provides reliable values of K_{M1} and k_{M1} , respectively associated with the formation and reactivity of the 1:1 alkali metal cation, POM anion pairs, M⁺·**1**. Calculated values for K_{M1} increase in the order $K_{\text{Li1}} = 21 \pm 10$, $K_{\text{Na1}} = 54 \pm 10$, and $K_{\text{K1}} = 65 \pm 6 \text{ M}^{-1}$ (uncertainties are 95% confidence intervals determined by statistical analysis of the nonlinear least-

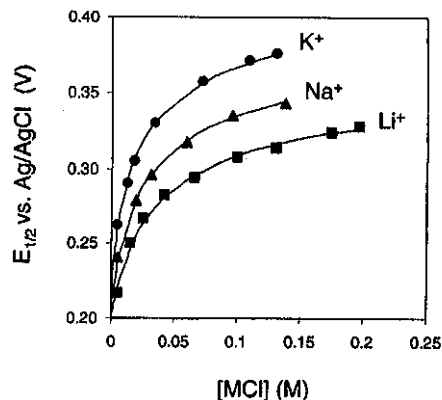


Figure 8. Plot of $E_{1/2}$ versus $[M^+]$ ($M^+ = \text{Li}^+, \text{Na}^+, \text{and K}^+$); $[M^+] = [\text{MCl}] + 5[\text{M}_5\text{I}] + [\text{MOAc}]$, $[\text{MCl}] = 0.0\text{--}0.2 \text{ M}$, $[\text{M}_5\text{I}] = 1.0 \text{ mM}$, $[\text{MOAc}] = 1 \text{ mM}$, $[\text{HOAc}] = 1 \text{ mM}$, 60°C , $E_{1/2}$ versus Ag/AgCl electrode. (Solid curves are from nonlinear least-squares fitting of the data to eq 42.)

squares regression data). The K_{M1} values increase as the size of the crystallographic radii of the cations become larger. Although electrostatic arguments dictate that K_{M1} values should decrease as the radii of the pairing ions become larger (see refs 84–85, below), the ordering of K_{M1} values reported here (discussed in detail below) is consistent with the formation of solvent-separated ion pairs (independent data in support of solvent-separated ion pairs is provided by ⁷Li NMR, below). As the crystallographic radii of the alkali metal cations increase, their charge densities decrease. Accordingly, the radii of the solvated cations decrease from Li⁺ to Na⁺ to K⁺.^{21,22,78,79} More significantly, now that ion pair stoichiometry and K_{M1} values have been quantified, the rectangular hyperbolic functional dependence of k_{obs} values on $[M^+]$ makes it possible to assign unique rate constants, k_{M1} , to the three M⁺·**1** pairs. These increase in the order $k_{\text{Li1}} = 0.065$, $k_{\text{Na1}} = 0.137$, and $k_{\text{K1}} = 0.225 \text{ M}^{-1} \text{ s}^{-1}$. The acquisition of rate constants for specific 1:1 ion pairs is an indispensable prerequisite to assessing the energetic and structural role of alkali metal cation size in electron transfer. These issues are now addressed by combined use of cyclic voltammetry, ⁷Li NMR, and chronoamperometry.

Energy of Electron Transfer to Solutions of 1:1 M⁺·**1** Pairs.

Cyclic voltammetry was used to measure the dependence of the reduction potentials ($E_{1/2}$ values) of solutions of **1** (1 mM) upon addition of alkali metal salts, MCl, $M^+ = \text{Li}^+, \text{Na}^+, \text{and K}^+$, under conditions identical to those used to obtain the k_{obs} data in Figure 7. For each cation, $E_{1/2}$ values for 1e⁻ reduction of V(V) in **1** to V(IV) (reduction of **1** to **1**_{red}) increased with $[M^+]$ (Figure 8; 22 $E_{1/2}$ values).

A fundamental distinction must be drawn between the kinetic data in Figure 7 and the thermodynamic data in Figure 8. As established above (Results and Discussion, part I), the rate of oxidation of BPH₂ by **1** is independent of $[\mathbf{1}_{\text{red}}]$. As a result,

(77) In the effective absence of ion pairing, a k_{obs} value of $(3.4 \pm 0.7) \times 10^{-3} \text{ M}^{-1} \text{ s}^{-1}$ (measured by using THA₅I and THAN, as described above, Figure 7) was obtained. The two systems (THA and alkali metal cations) differ in experimentally significant ways from one another: (1) the THA system uses a THA acetate buffer whose degree of self-association in the 2:3 water/*t*-BuOH solvent system differs from that of the alkali metal acetate buffers; (2) the extent and possible effect of interaction between THA and BPH₂ has not been quantified; and (3) in the effective absence of ion pairing between THA and **1** or **1**_{red}, the potential of the **1**/**1**_{red} couple is sufficiently negative that rapid back-reaction between **1**_{red} and BPH₂⁺⁺ prior to irreversible fragmentation of the successor complex, $[\text{BPH}_2^{++} - \mathbf{1}_{\text{red}}]$ cannot be excluded.

(78) Stern, K. H.; Amis, E. S. *Chem. Rev.* **1959**, *59*, 1–64.

(79) Sorensen, T. S.; Sloth, P.; Shroder, M. *Acta Chim. Scand.* **1984**, *A38*, 735–756.

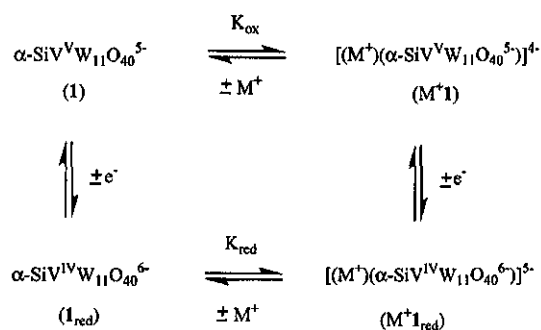
(73) Connors, K. A. *Binding Constants: The Measurement of Molecular Complex Stability*; John Wiley & Sons: New York, 1987; pp 59–69 and Appendix A, pp 373–384.

(74) Blackburn, R. L.; Hupp, J. T. *Chem. Phys. Lett.* **1988**, *150*, 399–405.

(75) $[M^+]$ values shown in Figure 7, and used to fit the data to eq 41, are the sum of $[M^+]$ from analytical (initially added) concentrations of MCl, POM counterions, and buffer. However, ion pairing between M⁺ and Cl⁻ is also possible. The association constant for the formation of M⁺Cl⁻ ion pairs, K_{MCl} , could be explicitly included in eq 41 by substituting $[\text{MCl}]/K_{\text{MCl}}[\text{Cl}^-]$ for $[M^+]$. At the same time, ion pairing of the added 1:1 alkali metal halide salts is but one of several phenomena that contribute to values of γ_M and is one reason γ_M is retained in eq 41. Values for the activity coefficient, γ_M , were calculated by using the extended Debye–Hückel law with a linear empirical correction term: $\log \gamma_z = -Az^2[\mu^{1/2}/(1 + Ba\mu^{1/2})] + b\mu$, where γ_z is the activity coefficient of a single ion of charge z , A ($1.825 \times 10^6(\epsilon T)^{-3/2} \text{ mol}^{-1/2} \text{ L}^{1/2} \text{ K}^{3/2}$) and B ($50.29(\epsilon T)^{-1/2} \text{ \AA}^{-1} \text{ mol}^{-1/2} \text{ L}^{1/2} \text{ K}^{1/2}$) are constants (ref 40, pp 230–231) that change with the temperature and dielectric constant of the solvent, and a and b are adjustable parameters. Values of A and B used to calculate the solid curves in Figure 7 were $A = 2.55 \text{ mol}^{-1/2} \text{ L}^{1/2} \text{ K}^{3/2}$ and $B = 0.563 \text{ \AA}^{-1} \text{ mol}^{-1/2} \text{ L}^{1/2} \text{ K}^{1/2}$. Values for a are approximated here by use of standard values (ref 39, p 47) commonly assigned to Li⁺, Na⁺, and K⁺ in water, and b was set equal to zero.

(76) Statistically meaningful support for the 1:1 stoichiometry in eq 39 requires measurement of k_{obs} values and agreement with the rectangular hyperbolic function (rate constant in eq 41) from 20 to 80% of complete saturation: (a) Deranleau, D. A. *J. Am. Chem. Soc.* **1969**, *91*, 4044. (b) Deranleau, D. A. *J. Am. Chem. Soc.* **1969**, *91*, 4050.

Scheme 1



the formation constant, K_{IP} , for pairing between M^+ and $\mathbf{1}_{\text{red}}$ is neither directly relevant to, nor available from, k_{obs} data. The situation is very different when measuring the reduction potentials of solutions of **1** in the presence of M^+ . Here, the standard Gibbs free energy of formation (ΔG_f°) values of all reactants and products of electron transfer from the electrode to solution contribute to the value of the $\mathbf{1}/\mathbf{1}_{\text{red}}$ couple.^{29,80} Species that must now be considered include **1** and $\text{M}^+\mathbf{1}$, $\mathbf{1}_{\text{red}}$ and $\text{M}^+\mathbf{1}_{\text{red}}$ ^{80b-c} (Scheme 1; following convention, K_{IP} for formation of $\text{M}^+\mathbf{1}$ is labeled K_{ox} , while K_{IP} for formation of $\text{M}^+\mathbf{1}_{\text{red}}$ is labeled K_{red}).

Accordingly, the Nernstian expression describing the dependence of $E_{1/2}$ on $[\text{M}^+]$ includes both K_{ox} and K_{red} .^{39,81}

$$E_{1/2} = E_{1/2}^\circ + \frac{RT}{nF} \ln \left(\frac{1 + K_{\text{red}}[\text{M}^+]\gamma_{\text{M}}}{1 + K_{\text{ox}}[\text{M}^+]\gamma_{\text{M}}} \right) + \frac{RT}{nF} \ln \left(\frac{\gamma_{\text{ox}}}{\gamma_{\text{red}}} \right) \quad (42)$$

In the absence of absolute values for K_{red} or K_{ox} , eq 42 can, at best, provide information about $K_{\text{red}}/K_{\text{ox}}$ ratios. Notably, however, the K_{M1} values calculated by using the data in Figure 7 and eq 41 (i.e., 21, 54, and 65 M^{-1} , respectively, for KLi1 , KNa1 , and KK1) correspond to the K_{ox} values in Scheme 1 and eq 42. Thus, combination of the kinetic (k_{obs}) data in Figure 7 with the thermodynamic ($E_{1/2}$) data in Figure 8 provides access to information (K_{red} values) not readily obtained by either approach alone.

K_{red} values associated with the three alkali metal cations, i.e., KLi1_{red} , KNa1_{red} , and KK1_{red} , were calculated by simultaneous nonlinear least-squares fitting of all the data in Figure 8 to eq 42. The result is shown by the solid curves in Figure 8. To minimize the number of adjustable parameters, only the most essential activity coefficients, i.e., those included⁵² in eq 42 (γ_{M} , γ_{ox} , and γ_{red}), were used. Moreover, the same Debye–Hückel parameters used to calculate γ_{M} in eq 41 were also used here to calculate γ_{ox} and γ_{red} .⁸³ The calculation was performed with the stipulation that the three curves in Figure 8 converge

(80) (a) Lexa, D.; Rentien, P.; Savéant, J.-M.; Xu, F. *J. Electroanal. Chem.* **1985**, *191*, 253–279. (b) Way, D. M.; Cooper, J. B.; Sadek, M.; Vu, T.; Mahon, P. J.; Bond, A. M.; Brownlee, R. T. C.; Wedd, A. G. *Inorg. Chem.* **1997**, *36*, 4227–4233. (c) Way, D. M.; Bond, A. M.; Wedd, A. G. *Inorg. Chem.* **1997**, *36*, 2826–2833. (d) Prenzler, P. D.; Boskovic, C.; Bond, A. M.; Wedd, A. G. *Anal. Chem.* **1999**, *71*, 3133–3139. (e) Bond, A. M.; Vu, T.; Wedd, A. G. *J. Electroanal. Chem.* **2000**, *494*, 96–104.

(81) In previous work (ref 21), a rectangular hyperbolic function was used to model the dependence of $E_{1/2}$ on $K_{\text{M1}}[\text{M}^+]$. While not rigorously correct, the rectangular hyperbolic function served as a practically useful and internally consistent method for establishing ion pair stoichiometry. Equation 42, however, not only is more rigorously correct, but also provides values for both K_{M1} and $K_{\text{M1}_{\text{red}}}$.

(82) The coefficient γ_{M} is associated with $[\text{M}^+]$, a quantity that is varied over a wide range of values; γ_{ox} and γ_{red} are experimentally significant and, from a purely mathematical perspective, $E_{1/2}$ values possess a significant functional dependence on $(RT/F) \ln(\gamma_{\text{ox}}/\gamma_{\text{red}})$.

to a single value, $E_{1/2} = E_{1/2}^\circ$, as $[\text{M}^+]$ approaches zero. The excellent fit (solid curves in Figure 8) provides independent support for the K_{M1} values calculated from the kinetic data in Figure 7. Calculated $K_{\text{M1}_{\text{red}}}$ values are as follow: for $\text{M}^+ = \text{Li}^+$, $130 \pm 30 \text{ M}^{-1}$; for Na^+ , $570 \pm 120 \text{ M}^{-1}$; and for K^+ , $2000 \pm 300 \text{ M}^{-1}$ (uncertainties are 95% confidence intervals determined by statistical analysis of the nonlinear least-squares regression data).

The formation constants K_{M1} increase with size (crystallographic radii) of the M^+ ions. According to the Eigen–Fuoss model^{84,85} for tight association between hard spheres (contact ion pairs) in an unstructured dielectric continuum, K_{IP} values possess an inverse exponential dependence on the distance, d (actually $d^3 e^{1/d}$), between the centers of the two paired ions. Accordingly, the increase in K_{M1} values from Li^+ to K^+ suggests that d values decrease as the crystallographic radii of the cations become larger. To the extent that the straightforward electrostatic arguments used to derive the Eigen–Fuoss model apply, the increase in K_{M1} values suggests the formation of solvent-separated ion pairs within which the solvated radii of the cations decrease from Li^+ to K^+ .⁸⁶ Upon reduction of **1** to $\mathbf{1}_{\text{red}}$, formation constants increase by factors ($K_{\text{M1}_{\text{red}}}/K_{\text{M1}}$) of ca. 6 for Li^+ , 11 for Na^+ , and 31 for K^+ . Again consistent with the effect of Coulombic attraction between ions in solvent-separated pairs, the increase in K values, as the charge product z_1z_2 increases from 5– to 6–, is greater for the more tightly associated ion pairs of the less highly solvated cations.

Solvent-Separated Ion Pairs. Ion pairing between Li^+ and **1** was demonstrated by the functional dependence of ^7Li NMR chemical shift values on the total concentration of $\text{Li}_3\mathbf{1}$ (Figure 9a). Evidence that these pairs are solvent separated was then provided by the small value of the molar paramagnetic contact shift (d) in ^7Li NMR spectra paramagnetic solutions of $\mathbf{1}$ -reduced $\text{Li}_6\mathbf{1}_{\text{red}}$ (Figure 9b).^{87,88}

Eight solutions of $\text{Li}_3\mathbf{1}$, varying in concentration from 0.3 to 15 mM in **1** (1.5–75 mM Li^+) were prepared in 2:3 (v/v) $\text{H}_2\text{O}/t\text{-BuOH}$ and heated to 60.0 °C in the NMR probe. Exchange between free Li^+ ions and those paired to **1** is sufficiently rapid on the NMR time scale that a single ^7Li NMR signal is observed (rapid exchange limit). The chemical shift of this signal moves downfield as the fraction of Li^+ paired to **1** gradually increases with $[\text{Li}_3\mathbf{1}]$. The data in Figure 9a are consistent with effectively

(83) The extended Debye–Hückel law with a linear empirical correction term was used. The same values of A , B and a (for Li^+ , Na^+ , and K^+) as those listed above in ref 39 (p 47) were used as well, while b was now allowed to vary. Values of a used as starting points (prior to nonlinear regression) to calculate γ_{ox} and γ_{red} were averages of published effective hydrodynamic radii of **1**, a 5– anion, and of $\text{AlVW}_{11}\text{O}_{40}^{6-}$, a 6– anion, obtained from diffusion coefficient data under conditions (solvent, temperature, added salts) identical to those used here (see ref 21). Final values (after nonlinear fitting) were in a similar range: 4.66 Å for a in calculating γ_{ox} and 6.16 Å for a in calculating γ_{red} .

(84) $K = (4\pi N d^3 / 3000) \exp(-U_{(d)}/RT)$, where $U_{(d)} = z_1 z_2 e^2 / \{D_s d(1 + \chi d)\}$; $\chi = (8\pi N e^2 \mu / 1000 D_s RT)^{1/2}$ (from ref 85).

(85) Billing, R.; Rehorek, D.; Henning, H. In *Photoinduced Electron Transfer in Ion Pairs*; Mattay, J., Ed.; Springer-Verlag: Berlin, 1990; Vol. 158.

(86) The Eigen–Fuoss model gives $K_{\text{Li1}} = 230 \text{ M}^{-1}$ (a d value of 8.3 Å for 1 mM $\text{Li}_3\mathbf{1}$ in 202 mM LiCl , $\mu = 2.17 \times 10^{-4} \text{ mol/cm}^3$, was estimated by using effective hydrodynamic radii of the ion pairs, r_{eff} , published in ref 21, and taking $d = r_{\text{eff}}$). Analogous calculations give $K_{\text{Na1}} = 482 \text{ M}^{-1}$ ($d = 7.7$ Å for 1 mM $\text{Na}_3\mathbf{1}$ in 110 mM NaCl , $\mu = 1.25 \times 10^{-4} \text{ mol/cm}^3$) and $K_{\text{K1}} = 2145 \text{ M}^{-1}$ ($d = 6.8$ Å for 1 mM $\text{K}_3\mathbf{1}$ in 85 mM KCl , $\mu = 1.00 \times 10^{-4} \text{ mol/cm}^3$). Concentrations of added M^+ (Li^+ , Na^+ and K^+) were estimated, on the basis of experimental K_{IP} values, to give solutions containing 93% 1:1 paired $\text{M}^+\mathbf{1}$.

(87) Screttas, C. G.; Heropoulos, G. A.; Steele, B. R.; Bethell, D. *Magn. Reson. Chem.* **1998**, *36*, 656–662.

(88) Micha-Screttas, M.; Heropoulos, G. A.; Steele, B. R. *J. Chem. Soc., Perkin Trans. 2* **1999**, *1999*, 1443–1446.

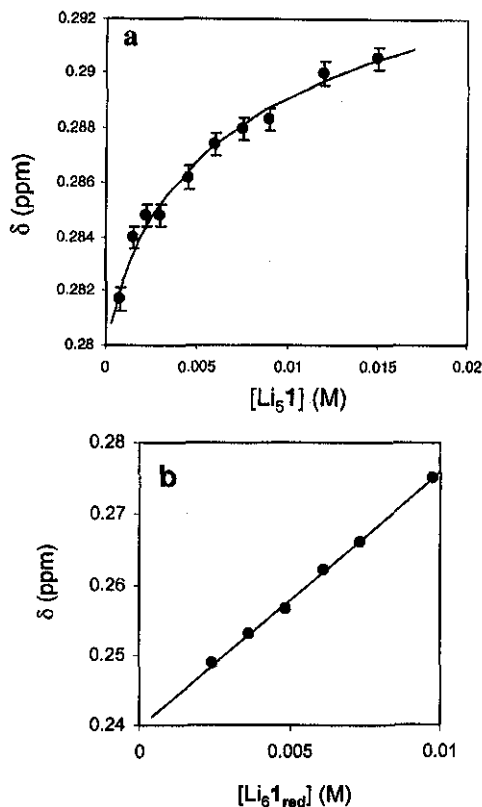


Figure 9. (a) Chemical shift of the ${}^7\text{Li}$ NMR signal (relative to 1.0 M LiCl in D_2O) as the concentration of Li_3I is increased from 0.3 to 15 mM (1.5–75 mM Li^+) in 2:3 (v/v) $\text{H}_2\text{O}/t\text{-BuOH}$ at 60 $^\circ\text{C}$. A digital resolution of 0.061 Hz (0.0004 ppm) was used to accurately measure the relatively small changes in chemical shift values. Solid curve: nonlinear least-squares fit to eq 28 (see Experimental Section); $\delta_0 = 0.287$ ppm, $\delta_1 = 0.336$ ppm, $K_{\text{LiI}} = 65 \pm 35 \text{ M}^{-1}$ (95% confidence interval). (b) Chemical shift of the ${}^7\text{Li}$ NMR signal as the concentration of $\text{Li}_6\text{I}_{\text{red}}$ is increased from 0.5 to 10 mM in 2:3 (v/v) $\text{H}_2\text{O}/t\text{-BuOH}$ at 60 $^\circ\text{C}$. The slope ($\Delta\delta_{\text{obs}} \text{ M}^{-1}$) is 3.62 ppm M^{-1} ($R^2 = 0.998$).

no ion pairing at the low concentration limit (1.5 mM Li^+ and 0.3 mM I) and the formation of 1:1 ion pairs, Li^+I , as $[\text{Li}_3\text{I}]$ increases. At each $[\text{Li}_3\text{I}]$, the chemical shift of the ${}^7\text{Li}$ NMR signal is a weighted mean of contributions from unpaired and paired Li^+ ions. A nonlinear least-squares fit of the data to a model expressing the change in chemical shift for the 1:1 association reaction in eq 39 as a function of the $[\text{Li}_3\text{I}]$ (see eq 28, Experimental Section) gives a formation constant (K_{LiI} value) of $65 \pm 35 \text{ M}^{-1}$ (uncertainty is a statistically determined 95% confidence interval). Despite the very small range of δ values, the K_{LiI} value calculated from these data is nonetheless within statistical uncertainty of that obtained independently from k_{obs} data (i.e., 21 ± 10).

Once it was demonstrated that the ${}^7\text{Li}$ NMR technique gave a reasonable value for K_{LiI} , spectra of paramagnetic solutions of the le–reduced complex, $\text{Li}_6\text{I}_{\text{red}}$, were obtained (Figure 9b). The chemical shift of the ${}^7\text{Li}$ NMR signal (δ_{obs}) increases linearly with the concentration of paramagnetic $\text{Li}_6\text{I}_{\text{red}}$. The observed chemical shift value⁸⁷ is a linear combination of contributions from bulk susceptibility (δ_{bulk} , a concentration-dependent result of macroscopic interactions) and contact shift, δ_{c} , that arises from spin density transfer from a paramagnetic center (e.g., V(IV) in I_{red}):

$$\delta_{\text{obs}} = \delta_{\text{bulk}} + 2\delta_{\text{c}} \quad (43)$$

In the case of rapid exchange, δ_{c} is also concentration dependent.

In the present case, therefore, both δ_{bulk} and δ_{c} must be evaluated as molar values (ppm M^{-1}).⁸⁸ From the data in Figure 9b ($\delta_{\text{obs}} = 3.62$ ppm M^{-1}), values of $\delta_{\text{bulk}} = 4.72$ and $\delta_{\text{c}} = -0.55$ ppm M^{-1} are obtained (333 K and $s = 1/2$, i.e., one unpaired electron).⁸⁷ An absence or only a very small contribution of δ_{c} to δ_{obs} suggests that the paired ions (whose formation is shown in Figure 9a) are substantially electronically insulated from one another by solvent and, hence, likely exist in solution as solvent-separated ion pairs.⁸⁸

Relative Sizes of the Solvent-Separated Ion Pairs, M^+I ($\text{M}^+ = \text{Li}^+, \text{Na}^+, \text{K}^+$). Relative molecular volumes of the 1:1 pairs were compared as *effective* hydrodynamic radii. These radii were estimated by using the Stokes–Einstein equation: $D = kT/6\pi\eta r$ (D is the diffusion coefficient of a sphere of radius r in a solvent of viscosity η).^{89–91} The viscosity of 2:3 (v/v) $\text{H}_2\text{O}/t\text{-BuOH}$ at 60 $^\circ\text{C}$ was measured by using a capillary viscometer. Concentrations of Li^+ , Na^+ , and K^+ required to prepare solutions containing 93% 1:1 paired and 7% unpaired I were determined by mass balance ($[\text{M}^+\text{I}]/[\text{I}] = K_{\text{MI}}[\text{M}^+]$) using the K_{MI} values listed in Table 3 (below). (LiCl (202 mM), NaCl (110 mM), and KCl (85 mM), respectively, were added to 1.0 mM solutions of Li_3I , Na_3I , and K_3I .) Diffusion coefficients, D , of the three 1:1 ion pairs, Li^+I , Na^+I , and K^+I , were then determined by single-potential step chronoamperometry.²¹ While the absolute values of radii assigned to Li^+I , Na^+I , and K^+I must be regarded as approximate, Stokes–Einstein provides an internally consistent means for comparing the relative molecular volumes associated with specific diffusion coefficient, D , values.^{92,93}

In pure water as solvent, the diffusion coefficients of solutions of I (MCl concentrations corresponding to the plateau regions in Figure 7) are the same for added LiCl, NaCl, or KCl and all give the same Stokes–Einstein radius, $5.6 \pm 0.2 \text{ \AA}$, as that reported for the unpaired Keggin ions in water (i.e., 5.6 \AA , for $\text{PW}_{12}\text{O}_{40}^{3-}$ and for $\text{SiW}_{12}\text{O}_{40}^{4-}$).⁹⁴ In 2:3 (v/v) $\text{H}_2\text{O}/t\text{-BuOH}$ at 60 $^\circ\text{C}$, however, 1:1 ion pairing occurs. Now, the diffusion coefficients and effective Stokes–Einstein radii decrease as the crystallographic radii of the alkali metal cations become larger (Table 3, below). Crystallographic (Shannon and Prewitt) radii of hexacoordinate Li^+ , Na^+ , and K^+ ions increase, respectively, from 0.90 to 1.16 to 1.52 A .⁹⁵ However, the solvated radii of these ions decrease with charge density, e/r , in the same order.^{78,96,97} Thus, the volumes of the solvated cations, and hence the effective hydrodynamic radii of the solvent-separated 1:1 ion pairs, decrease as the radii of the “naked” alkali metal cations become larger.

Role of Alkali Metal Cation Size in the Energy and Rate of Electron Transfer to Solvent-Separated Ion Pairs, M^+I ($\text{M}^+ = \text{Li}^+, \text{Na}^+, \text{K}^+$). The outer-sphere electron-transfer

(89) Hydrodynamic (Stokes–Einstein) radii of Keggin anions estimated from diffusion coefficient data match those obtained by velocity ultracentrifugation and from viscosity and density data (refs 90 and 91).

(90) Baker, M. C.; Lyons, P. A.; Singer, S. J. *J. Am. Chem. Soc.* **1955**, *77*, 2011–2012.

(91) Kurucsev, T.; Sargeson, A. M.; West, B. O. *J. Phys. Chem.* **1957**, *61*, 1567–1569.

(92) The Stokes–Einstein equation has been used successfully to provide meaningful “average” radii when applied to nonspherical (but similarly shaped) ions (ref 93).

(93) Edward, J. T. *J. Chem. Educ.* **1970**, *47*, 261–70.

(94) Pope, M. T.; Varga, G. M., Jr. *Inorg. Chem.* **1966**, *5*, 1249–1254.

(95) Shannon, R. D.; Prewitt, C. T. *Acta Crystallogr.* **1969**, *B25*, 925–46.

(96) The radii of hydrated Li^+ , Na^+ , and K^+ ions in water decrease from ca. 3.40 to 2.76 to 2.32 A as the waters of hydration decrease from ca. 25.3 to 16.6 to 10.5 (ref 97).

(97) Cotton, F. A.; Wilkinson, G. *Advanced Inorganic Chemistry*, 4th ed.; Wiley: New York, 1980; p 255.

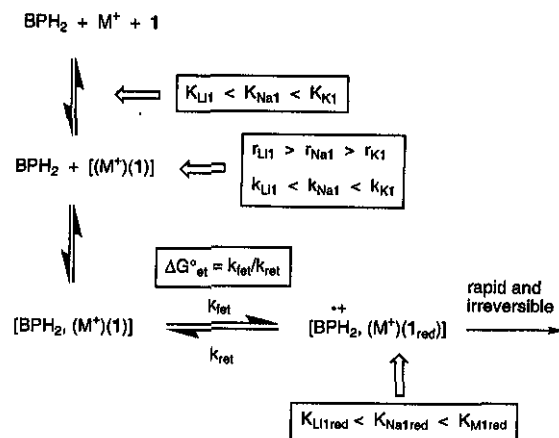
Table 3. Formation and Solution Properties of 1:1 Solvent-Separated Ion Pairs^a [(M⁺)(SiV^{IV}W₁₁O₄₀)]⁴⁻ (M⁺1) and [(M⁺)(SiV^{IV}W₁₁O₄₀)]⁵⁻ (M⁺1_{red})

cation, M ⁺	<i>r</i> _{eff} , Å ^b	<i>K</i> _{M1} (M ⁻¹)	<i>k</i> _{M1} (M ⁻¹ s ⁻¹)	<i>E</i> _{1/2} (mV) ^{b,c}	<i>K</i> _{M1red} (M ⁻¹)
Li ⁺	8.3 ± 0.4	21 ± 10	0.065 ± 0.013	327	130 ± 30
Na ⁺	7.7 ± 0.2	54 ± 10	0.137 ± 0.011	338	570 ± 120
K ⁺	6.8 ± 0.3	65 ± 6	0.225 ± 0.010	362	2000 ± 300

^a H₂O/*t*-BuOH (2:3, v/v) at 60 °C. ^b 93% 1:1 paired and 7% unpaired **1** by addition of LiCl (202 mM), NaCl (110 mM), and KCl (85 mM), respectively, to 1.0 mM solutions of Li₅1, Na₅1, and K₅1. ^c Data from Figure 8 at 202 mM LiCl, 110 mM NaCl, and 85 mM KCl versus Ag/AgCl (3 M NaCl).

reaction of BPH₂ with **1** includes ion pairing, local ordering of solvent molecules, and steric and orientational constraints. These phenomena are not accounted for in the simplifying assumptions used to calculate key parameters in theoretical models, such as that of Marcus, that relate standard free energies of reaction, *DG*^o, to rates of electron transfer, *k*_{et}.^{17,98} In Marcus theory, the rate of electron transfer is a function of the energy associated with the formation of donor–acceptor precursor complexes (a Coulombic work term, *W*) and the reorganization energy, *I*, associated with subsequent changes in bond lengths and angles (of solvent and reactants) that lead to the transition state for electron transfer. In applications of this theory to the ideal case of electron transfer between spherical molecules in an unstructured dielectric continuum, the Coulombic work term, *W*, and the outer-sphere (solvent) reorganization energy, *I*_{out}, can both be calculated. While the inner-sphere reorganization energy, *I*_{in}, is less readily calculated, it can often be determined experimentally from reaction rate (self-exchange and cross reaction) data. In the reaction of **1** with BPH₂, however, the reactants are not only nonspherical, but are sterically hindered (BPH₂), and must be oriented so that local donor and acceptor sites are proximal to one another. In addition, changes in nuclear coordinates, *I* (both *I*_{in} and *I*_{out}), associated with the paired cation and its solvation sphere must be considered, and there is no readily applicable quantitative model for doing this. Related to this general problem is the fact that, even in stoichiometrically well characterized systems such as ours, the precise location of the paired cation within the donor–acceptor precursor complex is extraordinarily difficult to determine. As a result of these uncertainties, no comprehensive model describing the role of the alkali metal cations in electron transfer to ion pairs such as M⁺1 is available.

The absence of such a model⁹⁸ is due, in some part, to the difficulty encountered in efforts to determine the structure and physicochemical properties of specific ion pairs and to correlate these properties with reaction rate data. This problem is directly addressed by the data summarized in Table 3, which establish fundamental relationships between the physicochemical properties of solvent-separated M⁺1 pairs and fates of electron transfer. In Scheme 2, these relationships and properties are associated with the key species–M⁺1 pairs, as well as transient precursor and successor complexes—pertinent to assessing the energy (*DG*^o_{et}) and rate of electron transfer from BPH₂ to **1**. As the crystallographic radii of the alkali metal cations increase from 0.90 Å for Li⁺, 1.16 Å for Na⁺, to 1.52 Å, for K⁺, the effective hydrodynamic radii of the solvent-separated M⁺1 pairs decrease from 8.3 Å, for Li⁺1, 7.7 Å, for Na⁺1, to 6.8 Å for K⁺1. This trend in ion pair size parallels the decrease in the radii of the solvated M⁺ ions. Moreover, the decrease in ion pair size is reflected by an increase in formation constants, *K*_{M1}, as is

Scheme 2

expected on the basis of Coulombic arguments. These trends alone would account for the well-known observation that effectiveness in specific cation catalysis increases with alkali metal cation size: at equal [M⁺] values, a larger fraction of the acceptor anions is paired when M⁺ = K⁺ than when M⁺ = Li⁺.

At the same time, however, we are now in a position to compare the relative rates of oxidation of a common substrate by well-defined ion pairs differing only in the nature of M⁺. The rate constants, *k*_{M1}, associated with each ion pair are theoretical limiting values. They represent extrapolation of the kinetic data to the hypothetical case in which all the anions, **1**, present in solution exist as 1:1 pairs with M⁺. These rate constants, *k*_{M1}, increase in the order *k*_{Li1} = 0.065 < *k*_{Na1} = 0.137 < *k*_{K1} = 0.225 M⁻¹ s⁻¹. Meanwhile, the reduction potentials of solutions containing 93% paired and 7% unpaired **1** (listed in Table 3) increase substantially from Li⁺ to K⁺. As shown in Scheme 1, these thermodynamic values include Contributions from energies associated with the formation of M⁺1 pairs, with electron transfer itself (i.e., with reduction of V(V) in **1** to V(IV)), and with the concurrent formation of M⁺1_{red} pairs. As the size of M⁺ increases, the effective hydrodynamic radii of the 1:1 M⁺1 pairs (Table 3) decrease in size. On the basis of electrostatic arguments, reduction of the smaller, more intimate ion pairs is expected to be more energetically favorable. Moreover, analysis of electrochemical data reveals that, as M⁺ increases in size, *K*_{M1red} values increase dramatically. These increases in *K*_{M1red} values reflect increases in the energy (as *DG*^o_f = -*RT* ln *K*_{M1red}) associated with the formation of the M⁺1_{red} pairs. Thus, as M⁺ increases in size, the energy associated with ion pair formation makes a larger contribution to the standard free energy of reaction, *DG*^o_{rxn}. These increases in ion pairing energy are very likely reflected in the relative energies of reductions of M⁺1 pairs to M⁺1_{red} in the activated complex (i.e., in the electronic transitions [BPH₂, M⁺1] ® [BPH₂^{•+}, M⁺1_{red}]; Scheme 2). Thus, as M⁺1 pairs are reduced to M⁺1_{red} during electron transfer, contributions to *DG*^o_{et} (Scheme 2) associated with ion pairing itself (proportional to -*RT* ln(*K*_{M1red}/*K*_{M1})) increase with cation size. Using *K*_{M1red} and *K*_{M1} values from Table 3, contributions of ion pairing energy to *DG*^o_{et} increase with cation size: -*RT* ln(*K*_{M1red}/*K*_{M1}) (in kcal mol⁻¹) = -1.2 for Li⁺, -1.5 for Na⁺, and -2.3 for K⁺.

Undoubtedly, the changes in ion pairing energy realized upon reductions of M⁺1 to M⁺1_{red} include changes in solvation energy as well as changes in potential energy that are primarily electrostatic in origin. Furthermore, both of these energetic Contributions to *DG*^o_{et} involve changes in the relative positions of solvent molecules and ions. In addition, the precise effect of

changes in $\mathbf{DG}^{\circ}_{\text{et}}$ on the rate of electron transfer requires detailed information about these changes in nuclear coordinates (i.e., the reorganization energies, \mathbf{I} , associated with local changes in solvent structure and ion position). Ready assessment of such \mathbf{I} values is beyond the current level of theory. Nonetheless, for modestly favorable (negative) $\mathbf{DG}^{\circ}_{\text{et}}$ values, an increase in $|\mathbf{DG}^{\circ}_{\text{et}}|$ is generally associated with attenuation of the impact of \mathbf{I} on the magnitude of \mathbf{DG}^{\ddagger} (eq 44)^{20,99,100} and a commensurate increase in the rate of electron transfer.

$$\Delta G^{\ddagger} = W(r) + \frac{\lambda}{4} + \frac{\Delta G^{\circ\prime}}{2} + \frac{(\Delta G^{\circ\prime})^2}{4\lambda} \quad (44)$$

Conclusion

Combined kinetic (k_{M1} and K_{M1}), ⁷Li NMR spectroscopic (paramagnetic contact shift, \mathbf{d}_{c}), chronoamperometric (diffusion coefficients, D , and hydrodynamic radii, r_{eff}) and cyclic voltammetric ($K_{\text{M1,red}}$) data thus show that an increase in M^+ size results in the formation of smaller, more intimate solvent-separated ion

(99) Marcus, R. A. *Annu. Rev. Phys. Chem.* **1964**, *15*, 155–196.

(100) Ebersson, L. *Electron-Transfer Reactions in Organic Chemistry*; Springer-Verlag: Berlin, 1987.

pairs, $M^+\mathbf{1}$, that possess larger electron affinities (q/r) and suggest that, upon reduction of $M^+\mathbf{1}$ to $M^+\mathbf{1}_{\text{red}}$ in the activated complex, increases in ion pairing energy make increasingly larger contributions to $\mathbf{DG}^{\circ}_{\text{et}}$.

Acknowledgment. We thank Professor Fred C. Anson for useful input regarding some of the electrochemistry, Dr. Carl J. Houtman for nonlinear regression error analysis software, and the DOE (DE-FC36-95GO10090) (I.A.W. and C.L.H.) and the NSF (CHE-9412465) (C.L.H.) for support.

Supporting Information Available: Plot of log(initial rate = $d[\mathbf{1}_{\text{red}}]/dt$) versus log $[\mathbf{1}_{\text{red}}]$ (Figure S1); plot of log(initial rate) versus log [OAc⁻] (Figure S2); plot of ln(k_{obs}/T) versus $1/T$ (Figure S3); tabulated data used to estimate pK_{a} of 3,3',5,5'-tetra-*tert*-butylbiphenyl-4,4'-diol (BPH₂) in 2:3 (v/v) H₂O/*t*-BuOH at 60 °C (pK_{a} values of various phenols in water and in mixed water/alcohol solutions at several temperatures, Tables S1 and S2); derivation of eq 5 (PDF). This material is available free of charge via the Internet at <http://pubs.acs.org>.

JA010074Q